Tetranuclear and Octanuclear Manganese Carboxylate Clusters: Preparation and Reactivity of $(NBu^n_4)[Mn_4O_2(O_2CPh)_9(H_2O)]$ and Synthesis of $(NBu^n_4)_2[Mn_8O_4(O_2CPh)_{12}(Et_2mal)_2(H_2O)_2]$ with a "Linked-Butterfly" Structure

Michael W. Wemple,[1a] Hui-Lien Tsai,[1b] Sheyi Wang,[1a] Juan Pablo Claude,[1a] William E. Streib,[1a] John C. Huffman,[1a] David N. Hendrickson,*[,1b] and George Christou*[,1a]

Department of Chemistry and Molecular Structure Center, Indiana University, Bloomington, Indiana 47405-4001, and Department of Chemistry-0358, University of California at San Diego, La Jolla, California 92093-0358

Received March 20, 1996[⊗]

The reaction of $Mn(O_2CPh)_2{\cdot}2H_2O$ and $PhCO_2H$ in EtOH/MeCN with $NBu^n_4MnO_4$ gives $(NBu^n_4)[Mn_4O_2(O_2CPh)_9(H_2O)]$ (**4**) in high yield (85−95%). Complex **4** crystallizes in monoclinic space group $P2_1/c$ with the following unit cell parameters at −129 °C: $a = 17.394(3)$ Å, $b = 19.040(3)$ Å, $c = 25.660(5)$ Å, $\beta = 103.51(1)°$, $V = 8262.7$ Å^3, $Z = 4$; the structure was refined on F to R (R_w) = 9.11% (9.26%) using 4590 unique reflections with $F > 2.33\sigma(F)$. The anion of **4** consists of a $[Mn_4(\mu_3\text{-}O)_2]^{8+}$ core with a "butterfly" disposition of four Mn^{III} atoms. In addition to seven bridging $PhCO_2^-$ groups, there is a chelating $PhCO_2^-$ group at one "wingtip" Mn atom and terminal $PhCO_2^-$ and H_2O groups at the other. Complex **4** is an excellent steppingstone to other $[Mn_4O_2]$-containing species. Treatment of **4** with 2,2-diethylmalonate (2 equiv) leads to isolation of $(NBu^n_4)_2[Mn_8O_4(O_2CPh)_{12}(Et_2mal)_2(H_2O)_2]$ (**5**) in 45% yield after recrystallization. Complex **5** is mixed-valent ($2Mn^{II},6Mn^{III}$) and contains an $[Mn_8O_4]^{14+}$ core that consists of two $[Mn_4O_2]^{7+}$ ($Mn^{II},3Mn^{III}$) butterfly units linked together by one of the μ_3-O^{2-} ions in each unit bridging to one of the body Mn atoms in the other unit, and thus converting to μ_4-O^{2-} modes. The Mn^{II} ions are in wingtip positions. The Et_2mal^{2-} groups each bridge two wingtip Mn atoms from different butterfly units, providing additional linkage between the halves of the molecule. Complex **5**·$4CH_2Cl_2$ crystallizes in monoclinic space group $P2_1/c$ with the following unit cell parameters at −165 °C: $a = 16.247(5)$ Å, $b = 27.190(8)$ Å, $c = 17.715(5)$ Å, $\beta = 113.95(1)°$, $V = 7152.0$ Å^3, $Z = 4$; the structure was refined on F to R (R_w) = 8.36 (8.61%) using 4133 unique reflections with $F > 3\sigma(F)$. The reaction of **4** with 2 equiv of bpy or picolinic acid (picH) yields the known complex $Mn_4O_2(O_2CPh)_7(bpy)_2$ (**2**), containing $Mn^{II},3Mn^{III}$, or $(NBu^n_4)[Mn_4O_2(O_2CPh)_7(pic)_2]$ (**6**), containing $4Mn^{III}$. Treatment of **4** with dibenzoylmethane (dbmH, 2 equiv) gives the mono-chelate product $(NBu^n_4)[Mn_4O_2(O_2CPh)_8(dbm)]$ (**7**); ligation of a second chelate group requires treatment of **7** with Na(dbm), which yields $(NBu^n_4)[Mn_4O_2(O_2CPh)_7(dbm)_2]$ (**8**). Complexes **7** and **8** both contain a $[Mn_4O_2]^{8+}$ ($4Mn^{III}$) butterfly unit. Complex **7** contains chelating dbm^- and chelating $PhCO_2^-$ at the two wingtip positions, whereas **8** contains two chelating dbm^- groups at these positions, as in **2** and **6**. Complex **7**·$2CH_2Cl_2$ crystallizes in monoclinic space group $P2_1$ with the following unit cell parameters at −170 °C: $a = 18.169(3)$ Å, $b = 19.678(4)$ Å, $c = 25.036(4)$ Å, $\beta = 101.49(1)°$, $V = 8771.7$ Å^3, $Z = 4$; the structure was refined on F to R (R_w) = 7.36% (7.59%) using 10 782 unique reflections with $F > 3\sigma(F)$. Variable-temperature magnetic susceptibility studies have been carried out on powdered samples of complexes **2** and **5** in a 10.0 kG field in the 5.0−320.0 K range. The effective magnetic moment (μ_{eff}) for **2** gradually decreases from 8.61 μ_B per molecule at 320.0 K to 5.71 μ_B at 13.0 K and then increases slightly to 5.91 μ_B at 5.0 K. For **5**, μ_{eff} gradually decreases from 10.54 μ_B per molecule at 320.0 K to 8.42 μ_B at 40.0 K, followed by a more rapid decrease to 6.02 μ_B at 5.0 K. On the basis of the crystal structure of **5** showing the single Mn^{II} ion in each $[Mn_4O_2]^{7+}$ subcore to be at a wingtip position, the Mn^{II} ion in **2** was concluded to be at a wingtip position also. Employing the reasonable approximation that $J_{wb}(Mn^{II}/Mn^{III}) = J_{wb}(Mn^{III}/M^{III})$, where J_{wb} is the magnetic exchange interaction between wingtip (w) and body (b) Mn ions of the indicated oxidation state, a theoretical χ_M *vs* T expression was derived and used to fit the experimental molar magnetic susceptibility (χ_M) *vs* T data. The obtained fitting parameters were $J_{wb} = -3.9$ cm^{-1}, $J_{bb} = -9.2$ cm^{-1}, and $g = 1.80$. These values suggest a $S_T = {}^5/_2$ ground state spin for **2**, which was confirmed by magnetization *vs* field measurements in the 0.5−50.0 kG magnetic field range and 2.0−30.0 K temperature range. For complex **5**, since the two bonds connecting the two $[Mn_4O_2]^{7+}$ units are Jahn−Teller elongated and weak, it was assumed that complex **5** could be treated, to a first approximation, as consisting of weakly-interacting halves; the magnetic susceptibility data for **5** at temperatures ≥40 K were therefore fit to the same theoretical expression as used for **2**, and the fitting parameters were $J_{wb} = -14.0$ cm^{-1} and $J_{bb} = -30.5$ cm^{-1}, with $g = 1.93$ (held constant). These values suggest an $S_T = {}^5/_2$ ground state spin for each $[Mn_4O_2]^{7+}$ unit of **5**, as found for **2**. The interactions between the subunits are difficult to incorporate into this model, and the true ground state spin value of the entire Mn_8 anion was therefore determined by magnetization *vs* field studies, which showed the ground state of **5** to be $S_T = 3$. The results of the studies on **2** and **5** are considered with respect to spin frustration effects within the $[Mn_4O_2]^{7+}$ units. Complexes **2** and **5** are EPR-active and -silent, respectively, consistent with their $S_T = {}^5/_2$ and $S_T = 3$ ground states, respectively.

Introduction

Over the last several years, we and others have been developing Mn carboxylate chemistry at the intermediate metal oxidation levels (II−IV) and at various nuclearities, and this has proven to be a fertile area. Complexes with nuclearities up to 18 have so far been obtained.[2−13] Our interest in this area stems from two sources: the desire to model the Mn_4 site

[⊗] Abstract published in *Advance ACS Abstracts,* October 1, 1996.

(1) (a) Indiana University. (b) University of California at San Diego.

(2) Lis, T. *Acta Crystallogr.* **1980**, *B36*, 2042.

S0020-1669(96)00301-1 CCC: $12.00 © 1996 American Chemical Society

of the photosynthetic water oxidation center (WOC) in green plants and cyanobacteria[14−20] and the growing recognition that Mn_x aggregates have a remarkable propensity to possess ground states with large spin (S) values.[18−29] The latter property appears to be a consequence of the presence within the Mn_x aggregate of (i) ferromagnetic exchange interactions between at least some of the Mn atoms[18,30] and/or (ii) spin frustration effects when $x \geq 3$ and the Mn atoms are arranged in an appropriate manner.[16,31,32]

One family of compounds that have been studied possess a $[Mn_4(\mu_3\text{-}O)_2]$ core with either a "butterfly" or planar disposition of the metal atoms. These have been obtained at three oxidation levels: $[Mn_4O_2(O_2CMe)_6(bpy)_2]$ (**1**; bpy = 2,2′-bipyridine) contains $2Mn^{II}$, $2Mn^{III}$ and a planar Mn_4 unit; $[Mn_4O_2(O_2CPh)_7(bpy)_2]$ (**2**) contains Mn^{II}, $3Mn^{III}$; and $[Mn_4O_2(O_2CR)_7(bpy)_2](ClO_4)$ (**3**; R = various) contains $4Mn^{III}$ and a butterfly Mn_4 unit.[15] With chelates other than bpy, only products at the $4Mn^{III}$ level have been obtained, possessing either a butterfly or a planar Mn_4 unit in $[Mn_4O_2(O_2CR)_7(L\text{-}L)_2]^-$ (L-L = picolinate (pic^-), 8-hydroxyquinolinate (hqn^-), the anion of 2-(hydroxymethyl)-pyridine (hmp^-), and the anion of dibenzoylmethane (dbm^-)) and $Mn_4O_2(O_2CR)_6(py)_2(dbm)_2$, respectively.[9,16,17,33] In parallel work, other groups have structurally-characterized the complexes $[Mn_4O_2(O_2CCPh_3)_6(Et_2O)_2]$, possessing $2Mn^{II}$, $2Mn^{III}$ and a planar Mn_4 unit,[34] and a number of $[Mn_4O_2]$-containing complexes where peripheral ligation is provided by polydentate N- or mixed N/O-based ligands; the latter complexes are all $4Mn^{III}$ with a planar disposition of Mn ions.[35−37]

Although **2** has eluded X-ray structural characterization, elemental analysis, IR spectroscopic data, and the similarity of **2** to **3** leave little doubt that it also has a butterfly Mn_4 unit;[15] however, assuming a trapped-valence nature as found in almost all mixed-valence Mn_x species containing Mn^{III} (and as also seen in **1**), the location of the Mn^{II} at a wingtip or body position of the butterfly has not been clear. Previously described are magnetochemical studies of **1** and **3** which indicate that they possess $S = 2$ and $S = 3$ ground states, respectively.[15] Detailed study of the $[Mn_4O_2]^{8+}$ complexes have shown that the $S = 3$ ground state is a result of spin frustration effects being operative in the core.[16]

More recently, efforts have turned toward the use of dicarboxylates in order to see how incorporation of this ligand type might affect the structures and physical properties of the products.[13,38,39] The first target complex was an $[Mn_4O_2]^{8+}$-containing species, and the dicarboxylate employed was 2,2-diethylmalonic acid (3,3-pentanedicarboxylic acid, Et_2malH_2) yielding the octanuclear complex $(NBu^n_4)_2[Mn_8O_4(O_2CPh)_{12}(Et_2mal)_2(H_2O)_2]$ (**5**). This work is herein described in full (a preliminary report[39] has appeared), together with a more detailed study of complex **2** than was previously presented; the latter study has also proven helpful in interpreting the magnetic properties of **5**. Also described are the preparation, structural characterization, and reactivity characteristics of $(NBu^n_4)[Mn_4O_2(O_2CPh)_9(H_2O)]$ (**4**), a "naked" butterfly complex with only carboxylate and H_2O peripheral ligation, representing a very convenient and reactive source of the $[Mn_4O_2]^{8+}$ unit. Portions of this work have been previously communicated.[7]

Experimental Section

Syntheses. All manipulations were performed under aerobic conditions using chemicals and solvents as received, except where otherwise noted. Elemental analyses were performed by Atlantic Microlab or

(3) Christmas, C.; Vincent, J. B.; Chang, H.-R.; Huffman, J. C.; Christou, G.; Hendrickson, D. N. *J. Am. Chem. Soc.* **1988**, *110*, 823.
(4) Luneau, D.; Savarinult, J.-M.; Tuchagues, J.-P. *Inorg. Chem.* **1988**, *27*, 3912.
(5) Bhula, R.; Weatherburn, D. C. *Angew. Chem., Int. Ed. Engl.* **1991**, *30*, 688.
(6) Low, D. W.; Eichhorn, D. M.; Draganescu, A.; Armstrong, W. H. *Inorg. Chem.* **1991**, *30*, 878.
(7) Wang, S.; Huffman, J. C.; Folting, K.; Streib, W. E.; Lobkovsky, E. B.; Christou, G. *Angew. Chem., Int. Ed. Engl.* **1991**, *30*, 1672.
(8) Gorun, S. M.; Stibrany, R. T. U.S. Patent 5,041,575, 1991.
(9) Wang, S.; Tsai, H.-L.; Streib, W. E.; Christou, G.; Hendrickson, D. N. *J. Chem. Soc., Chem. Commun.* **1992**, 677.
(10) Perlepes, S. P.; Huffman, J. C.; Christou, G. *J. Chem. Soc., Chem. Commun.* **1992**, 1657.
(11) Libby, E.; Folting, K.; Huffman, C. J.; Huffman, J. C.; Christou, G. *Inorg. Chem.* **1993**, *32*, 2549.
(12) Wang, S.; Tsai, H.-L.; Folting, K.; Martin, J. D.; Hendrickson, D. N.; Christou, G. *J. Chem. Soc., Chem. Commun.* **1994**, 671.
(13) Squire, R. C.; Aubin, S. M. J.; Folting, K.; Streib, W. E.; Christou, G.; Hendrickson, D. N. *Inorg. Chem.* **1995**, *34*, 6463.
(14) (a) Debus, R. J. *Biochim. Biophys. Acta* **1992**, *1102*, 269. (b) *Manganese Redox Enzymes*; Pecoraro, V. L., Ed.; VCH Publishers: New York, 1992.
(15) Vincent, J. B.; Christmas, C.; Chang, H.-R.; Li, Q.; Boyd, P. D. W.; Huffman, J. C.; Hendrickson, D. N.; Christou, G. *J. Am. Chem. Soc.* **1989**, *111*, 2086.
(16) Libby, E.; McCusker, J. K.; Schmitt, E. A.; Folting, K.; Hendrickson, D. N.; Christou, G. *Inorg. Chem.* **1991**, *30*, 3486.
(17) Bouwman, E.; Bolcar, M. A.; Libby, E.; Huffman, J. C.; Folting, K.; Christou, G. *Inorg. Chem.* **1992**, *31*, 5185.
(18) Hendrickson, D. N.; Christou, G.; Schmitt, E. A.; Libby E.; Bashkin, J. S.; Wang, S.; Tsai, H.-L.; Vincent, J. B.; Boyd, P. D. W.; Huffman, J. C.; Folting, K.; Li, Q.; Streib, W. E. *J. Am. Chem. Soc.* **1992**, *114*, 2455.
(19) Wang, S.; Tsai, H.-L.; Hagen, K. S.; Hendrickson, D. N.; Christou, G. *J. Am. Chem. Soc.* **1994**, *116*, 8376.
(20) Wemple, M. W.; Adams, D. M.; Folting, K.; Hendrickson, D. N.; Christou, G. *J. Am. Chem. Soc.* **1995**, *117*, 7275.
(21) Wemple, M. W.; Adams, D. M.; Hagen, K. S.; Folting, K.; Hendrickson, D. N.; Christou, G. *J. Chem. Soc., Chem. Commun.* **1995**, 1591.
(22) Caneschi, A.; Gatteschi, D.; Rey, P.; Sessoli, R. *Inorg. Chem.* **1991**, *30*, 3936.
(23) Caneschi, A.; Gatteschi, D.; Sessoli, R.; Barra, A. L.; Brunel, L. C.; Guillot, M. *J. Am. Chem. Soc.* **1991**, *113*, 5873.
(24) Sessoli, R.; Tsai, H.-L.; Schake, A. R.; Wang, S.; Vincent, J. B.; Folting, K.; Gatteschi, D.; Christou, G.; Hendrickson, D. N. *J. Am. Chem. Soc.* **1993**, *115*, 1804.
(25) Sessoli, R.; Gatteschi, D.; Caneschi, A.; Novak, M. A. *Nature* **1993**, *365*, 141.
(26) Vincent, J. B.; Tsai, H.-L.; Blackman, A. G.; Wang, S.; Boyd, P. D. W.; Folting, K.; Huffman, J. C.; Lobkovsky, E. B.; Hendrickson, D. N.; Christou, G. *J. Am. Chem. Soc.* **1993**, *115*, 12353.
(27) Eppley, H. J.; Tsai, H.-L.; de Vries, N.; Folting, K.; Christou, G.; Hendrickson, D. N. *J. Am. Chem. Soc.* **1995**, *117*, 301.
(28) Tsai, H.-L.; Wang, S.; Folting, K.; Streib, W. E.; Hendrickson, D. N.; Christou, G. *J. Am. Chem. Soc.* **1995**, *117*, 2503.
(29) Goldberg, D. P.; Caneschi, A.; Delfs, C. D.; Sessoli, R.; Lippard, S. J. *J. Am. Chem. Soc.* **1995**, *117*, 5789.
(30) Schmitt, E. A.; Noodleman, L.; Baerends, E. J.; Hendrickson, D. N. *J. Am. Chem. Soc.* **1992**, *114*, 6109.
(31) McCusker, J. K.; Tang, H. G.; Wang, S.; Christou, G.; Hendrickson, D. N. *Inorg. Chem.* **1992**, *31*, 1874.
(32) (a) McCusker, J. K.; Schmitt, E. A.; Hendrickson, D. N. In *Magnetic Molecular Materials*; Gatteschi, D., Kahn, O., Miller, J. S., Palacio, F., Eds.; Kluwer: Boston, 1991; pp 297−319. (b) Hendrickson, D. N. Spin Frustration in Polynuclear Complexes. In *Research Frontiers in Magnetochemistry*; O'Connor, C. J., Ed.; World Scientific: Singapore, 1993.
(33) Wang, S.; Folting, K.; Streib, W. E.; Schmitt, E. A.; McCusker, J. K.; Hendrickson, D. N.; Christou, G. *Angew. Chem., Int. Ed. Engl.* **1991**, *30*, 305.
(34) (a) Kulawiec, R. J.; Crabtree, R. H.; Brudvig, G. W.; Schulte, G. K. *Inorg. Chem.* **1988**, *27*, 1309. (b) Thorp, H. H.; Sarneski, J. E.; Kulawiec, R. J.; Brudvig, G. W.; Crabtree, R. H.; Papaefthymiou, G. C. *Inorg. Chem.* **1991**, *30*, 1153.
(35) (a) Mikuriya, M.; Yamato, Y.; Tokii, T. *Chem. Lett.* **1991**, 1429. (b) Mikuriya, M.; Yamato, Y.; Tokii, T. *Bull. Chem. Soc. Jpn.* **1992**, *65*, 2624.
(36) (a) Chandra, S. K.; Chakravorty, A. *Inorg. Chem.* **1991**, *30*, 3795. (b) Chandra, S. K.; Chakravorty, P.; Chakravorty, A. *J. Chem. Soc., Dalton Trans.* **1993**, 863.
(37) Gedye, C.; Harding, C.; McKee, V.; Nelson, J.; Patterson, J. *J. Chem. Soc., Chem. Commun.* **1992**, 392.
(38) Jiang, Z.-H.; Ma, S.-L.; Liao, D.-Z.; Yan, S.-P.; Wang, G.-L.; Yao, X.-K.; Wang, R.-J. *J. Chem. Soc., Chem. Commun.* **1993**, 745.
(39) Wemple, M. W.; Tsai, H.-L.; Streib, W. E.; Hendrickson, D. N.; Christou, G. *J. Chem. Soc., Chem. Commun.* **1994**, 1031.

the Microanalytical Laboratory, University of Manchester. (Et_2malH_2 = 2,2-diethylmalonic acid; bpy = 2,2′-bipyridine.) $NBu^n_4MnO_4$ was prepared as described elsewhere.[40] $Mn_4O_2(O_2CPh)_7(bpy)_2$ (**2**) was available from previous work.[15]

$Na_2(Et_2mal)$. Sodium metal (0.60 g, 26 mmol) was added in small portions to a solution of Et_2malH_2 (2.0 g, 12 mmol) in EtOH (60 mL) cooled in an ice bath. A white solid progressively precipitated from solution. When the reaction was complete, the slurry was stirred for a further 1 h, Et_2O (20 mL) added, and the white solid collected by filtration and washed copiously with Et_2O. The yield of $Na_2(Et_2mal)$ was 2.2 g (90%). ^1H NMR in D_2O solution (300 MHz, 23 °C): δ 1.58 (quartet, CH_2), 0.58 (triplet, CH_3). Anal. Calcd (found) for $C_7H_{10}O_4Na_2$: C, 41.19 (41.23); H, 4.94 (4.98); Na, 22.52 (22.62).

$Mn(O_2CPh)_2\cdot 2H_2O$. Separate solutions of NaO_2CPh (29.2 g, 202 mmol) in H_2O (150 mL) and of $MnCl_2\cdot 4H_2O$ (20.0 g, 101 mmol) in H_2O (100 mL) were mixed together at ∼80 °C with vigorous stirring. A light-pink crystalline solid precipitated immediately. The flask was stored in the refrigerator for 24 h, and the crystalline product was collected by filtration, washed with cold water, and dried in air; the yields were typically 53−66% (17.5−22.3 g). Anal. Calcd (found) for $C_{14}H_{14}O_6Mn$: C, 50.47 (50.36); H, 4.24 (4.17).

$(NBu^n_4)[Mn_4O_2(O_2CPh)_9(H_2O)]$ (4). To a stirred solution of $Mn(O_2CPh)_2\cdot 2H_2O$ (1.35 g, 4.05 mmol) and $PhCO_2H$ (3.75 g, 30.7 mmol) in a solvent mixture comprising EtOH (20 mL) and MeCN (10 mL) was added solid $NBu^n_4MnO_4$ (0.45 g, 1.25 mmol) in small portions. The resulting red-brown solution was evaporated to dryness and the residue redissolved in CH_2Cl_2 (15 mL) to give a dark-red solution. This was layered with a mixture of Et_2O (25 mL) and hexanes (25 mL). After several days, large needle-shaped crystals were formed; they were collected by filtration, washed with Et_2O, and dried in air; yield 85−95% (1.8−2.0 g). Anal. Calcd (found) for $C_{79}H_{83}NO_{21}Mn_4$: C, 59.22 (59.0); H, 5.22 (5.2); N, 0.87 (0.9); Mn, 13.71 (13.3). Electronic spectral data (CH_2Cl_2) [λ_{max}, nm (ϵ_M, $L\cdot mol^{-1}\cdot cm^{-1}$)]: 476 (11 560). IR data (Nujol, cm^{-1}): 3400 (w, br), 1609 (s), 1570 (s), 1522 (m), 1491 (m), 1305 (m), 1174 (m), 1068 (w), 1026 (m), 939 (w), 858 (w), 837 (w), 719 (s), 677 (s), 665 (s), 605 (m), 472 (w).

$(NBu^n_4)_2[Mn_8O_4(O_2CPh)_{12}(Et_2mal)_2(H_2O)_2]\cdot CH_2Cl_2$ (5·CH_2Cl_2). $Na_2(Et_2mal)$ (0.11 g, 0.54 mmol) was slowly dissolved with stirring over the course of 1 week in a solution of complex **4** (0.40 g, 0.25 mmol) in MeCN (25 mL). The resulting solution was then filtered to remove NaO_2CPh and unreacted $Na_2(Et_2mal)$, and the solvent was removed from the filtrate under vacuum. The brown solid residue was recrystallized twice from CH_2Cl_2/hexanes to give X-ray-quality, dark-brown crystals in ∼45% yield. Crystals kept in contact with the mother liquor to avoid solvent loss were identified crystallographically as **5**·$4CH_2Cl_2$; dried solid analyzed as **5**·CH_2Cl_2. Anal. Calcd (found) for $C_{131}H_{158}N_2O_{38}Cl_2Mn_8$: C, 54.65 (54.67); H, 5.53 (5.62); N, 0.97 (1.05). Selected IR data (Nujol, cm^{-1}): 3540 (w), 3063 (w), 1605 (s), 1572 (s), 1399 (s), 1319 (m), 1273 (m), 1175 (m), 1156 (m), 1142 (m), 1069 (m), 1026 (m), 839 (m), 714 (s), 689 (m), 679 (m), 621 (s), 473 (m).

Conversion of 4 to $Mn_4O_2(O_2CPh)_7(bpy)_2$ (2). A red-brown solution of complex **4** (0.40 g, 0.25 mmol) in THF (20 mL) was layered with a solution of bpy (0.080 g, 0.50 mmol) in MeCN (20 mL). A dark red-brown crystalline product formed after several days. This was collected by filtration, washed with Et_2O, and dried in air; yield 65%. The IR spectrum was identical with that of authentic material[15] except for the presence of THF bands. The solid analyzed as **2**·$^2/_3$THF. Anal. Calcd (found) for $C_{71.7}H_{56.3}N_4O_{16.7}Mn_4$: C, 58.95 (58.75); H, 3.88 (3.7); N, 3.84 (3.9); Mn, 15.04 (14.8). Use of only 1 equiv of bpy (0.25 mmol) leads to the same product but in decreased yield (∼30%).

Conversion of 4 to $(NBu^n_4)[Mn_4O_2(O_2CPh)_7(pic)_2]$ (6). A stirred red-brown solution of complex **4** (0.40 g, 0.25 mmol) in CH_2Cl_2 (20 mL) was treated with solid picolinic acid (0.062 g, 0.50 mmol). There was no significant change in color. From the resulting homogeneous solution, a crystalline product was precipitated in ∼90% (0.35 g) yield upon addition of Et_2O (40 mL). The solid was collected by filtration and washed with Et_2O. Recrystallization from CH_2Cl_2/(Et_2O + hexane) (1:1:1) gave well-formed crystals in 76% yield; these were collected by filtration, washed with Et_2O/hexanes, and dried in air. Their IR spectrum is identical with that of authentic complex **6**.[16] The solid analyzed for **6**·$^1/_2Et_2O$. Anal. Calcd (found) for $C_{79}H_{84}N_3O_{20.5}Mn_4$: C, 58.45 (58.2); H, 5.22 (4.85); N, 2.59 (2.6), Mn, 13.5 (13.2). The sample slowly lost weight during the elemental analysis.

Conversion of 4 to $(NBu^n_4)[Mn_4O_2(O_2CPh)_8(dbm)]$ (7). Method 1. Treatment of a red-brown solution of complex **4** (0.40 g, 0.25 mmol) in CH_2Cl_2 (15 mL) with solid dbmH (0.12 g, 0.50 mmol) gave a homogeneous dark-brown solution. This was layered with hexanes (20 mL). After several days, well-formed, dark-red crystals were collected by filtration, washed with Et_2O, and dried in air; yield 52−80% (0.24−0.37 g). The crystallographic studies indicated the formulation as **7**·$2CH_2Cl_2$; dried solid analyzed as **7**·CH_2Cl_2. Anal. Calcd (found) for $C_{88}H_{89}NO_{20}Cl_2Mn_4$: C, 59.67 (59.8); H, 5.06 (4.9); N, 0.79 (1.0); Mn, 12.41 (11.7). Selected IR data (Nujol): 1612 (s), 1572 (s), 1539 (s), 1520 (s), 1321 (s), 1304 (s), 1174 (m), 1068 (m), 1026 (m), 719 (s), 684 (s), 677 (s), 663 (s), 642 (m), 615 (m).

Method 2. To a red-brown solution of complex **4** (0.40 g, 0.25 mmol) in CH_2Cl_2 (15 mL) was added solid Na(dbm) (0.062 g, 0.25 mmol). The solution was stirred for several hours until all the Na(dbm) had reacted. The precipitate (NaO_2CPh) was removed by filtration, and the filtrate was layered with hexanes (25 mL). Several days later, crystals of **7** were collected by filtration, washed with Et_2O, and dried in air; yield 70−79%. The IR spectrum is identical with that for the sample prepared by method 1.

Conversion of 7 to $(NBu^n_4)[Mn_4O_2(O_2CPh)_7(dbm)_2]$ (8). A slurry of complex **7** (0.35 g, 0.20 mmol) and Na(dbm) (0.050 g, 0.20 mmol) in CH_2Cl_2 (15 mL) was stirred for 4 h. A precipitate of NaO_2CPh was removed by filtration. The brown filtrate was treated with Et_2O (15 mL) and hexanes (15 mL) to give a brown precipitate, and the latter was collected by filtration, washed with Et_2O, and dried in air; yield 0.18 g (50%). The IR spectrum of this compound is identical with that of authentic material.[19,41]

Conversion of 8 to 6. Complex **8** (0.18 g, 0.10 mmol) was dissolved in CH_2Cl_2 (10 mL), and solid picolinic acid (0.028 g, 0.22 mmol) was added with stirring. No noticeable color change occurred. After 30 min, Et_2O (10 mL) and hexanes (20 mL) were added, precipitating a reddish-brown crystalline solid, which was collected by filtration, washed with Et_2O, and dried in air; yield 85%. The IR spectrum of this solid was identical with that of authentic complex **6**.[16] Use of Na(pic) in place of picH also gave complex **6**; yield 66%.

X-ray Crystallography and Structure Solution. Data for complexes **4**, **5**·$4CH_2Cl_2$, **7**·$2CH_2Cl_2$ were collected on a Picker four-circle diffractometer at approximately −129, −165, and −170 °C, respectively; details of the diffractometry, low-temperature facilities, and computational procedures employed by the Molecular Structure Center are available elsewhere.[42] The crystals were covered with silicone grease (for **5**·$4CH_2Cl_2$ and **7**·$2CH_2Cl_2$, this prevented rapid solvent loss observed in crystals that did not diffract) and affixed to glass fibers, mounted on a goniometer head, and placed in a nitrogen cold stream for characterization. Data collection parameters ($+h,+k,\pm l$; $6° \geq 2\theta \leq 45°$) are summarized in Table 1.

For all complexes, a systematic search of a limited hemisphere of reciprocal space revealed a primitive monoclinic cell. Following complete intensity data collection, the conditions $l = 2n$ for $h0l$ and $k = 2n$ for $0k0$ uniquely determined the space group as $P2_1/c$ for **4** and **5**·$4CH_2Cl_2$. For **7**·$2CH_2Cl_2$, the only observed condition was $k = 2n$ for $0k0$, and after an initial unsuccessful attempt in space group $P2_1/m$, the structure was solved by assuming space group $P2_1$. Data processing gave residuals of 0.078, 0.147, and 0.025 for **4**, **5**·$4CH_2Cl_2$, and **7**·$2CH_2Cl_2$, respectively, for the averaging of 3277, 2482, and 4421 unique intensities that had been measured more than once. Although the residual for **5**·$4CH_2Cl_2$ is larger than normally expected, it was a weak data set; of 9371 total unique intensities, only 4133 had $F > 3\sigma(F)$. Four standards measured every 300 reflections showed no consistent trends. No corrections were made for absorption.

The structures were solved using a combination of direct methods (MULTAN78) and Fourier techniques. The positions of the Mn atoms

(40) Vincent, J. B.; Chang, H.-R.; Folting, K.; Huffman, J. C.; Christou, G.; Hendrickson, D. N. *J. Am. Chem. Soc.* **1987**, *109*, 5703.

(41) Wang, S.; Tsai, H.-L.; Wemple, M. W.; Hagen, K. S.; Hendrickson, D. N.; Christou, G. Manuscript in preparation.

(42) Chisholm, M. H.; Folting, K.; Huffman, J. C.; Kirkpatrick, C. C. *Inorg. Chem.* **1984**, *23*, 1021.

Table 1. Crystallographic Data for Complexes **4**, **5**·4CH_2Cl_2, and **7**·2CH_2Cl_2

	4	**5**·4CH_2Cl_2	**7**·2CH_2Cl_2
formula[a]	$C_{79}H_{83}NO_{21}Mn_4$	$C_{134}H_{164}N_2O_{38}Cl_8Mn_8$	$C_{89}H_{91}NO_{20}Cl_4Mn_4$
fw	1602.27	3133.88	1856.26
space group	$P2_1/c$	$P2_1/c$	$P2_1$
a, Å	17.394(3)	16.247(5)	18.169(3)
b, Å	19.040(3)	27.190(8)	19.678(4)
c, Å	25.660(5)	17.715(5)	25.036(4)
β, deg	103.51(1)	113.95(1)	101.49(1)
V, Å^3	8262.7	7152.0	8771.7
Z	4	2	4
T, °C	−129	−165	−170
λ, Å[b]	0.71069	0.71069	0.71069
ρ_{calc}, g/cm^3	1.288	1.455	1.406
μ, cm^{-1}	6.380	8.798	7.297
octants	$+h,+k,\pm l$	$+h,+k,\pm l$	$+h,+k,\pm l$
no. of obsd data	4590[c]	4133[d]	10 782[d]
R (R_w), %[e,f]	9.11 (9.26)	8.36 (8.61)	7.36 (7.59)

[a] Including solvate molecules. [b] Mo Kα; graphite monochromator. [c] $F > 2.33\sigma(F)$. [d] $F > 3.0\sigma(F)$. [e] $R = 100\sum||F_o| - |F_c||/\sum|F_o|$. [f] $R_w = 100[\sum w(|F_o| - |F_c|)^2/\sum w|F_o|^2]^{1/2}$ where $w = 1/\sigma^2(|F_o|)$.

were obtained from initial E maps. The positions of the remaining non-hydrogen atoms were obtained from subsequent iterations of least-squares refinement and difference Fourier maps phased on the already-located atoms. For **4**, the asymmetric unit contains a complete anion and cation pair. For **5**·4CH_2Cl_2, the asymmetric unit contains half the Mn(8) anion, one $NBu^n_4{}^+$ cation, and two molecules of solvent CH_2Cl_2; one CH_2Cl_2 molecule refined to essentially full occupancy while the other refined to an occupancy of approximately 75%, and these occupancies were fixed for the remainder of the refinement. There is large thermal motion for some of the atoms, notably some of the CH_3 carbon atoms in the butyl groups of the cations of **4** and **5**·4CH_2Cl_2 and in the malonate ligand of the latter. Hydrogen atoms were included in fixed, calculated positions in both structures, except those of the bound water molecules. Hydrogen thermal parameters were fixed at 1 plus the isotropic thermal parameters of the atoms to which they were bonded. For **7**·2CH_2Cl_2, the asymmetric unit contains two independent Mn_4 anions, two $NBu^n_4{}^+$ cations, and four molecules of partial-occupancy CH_2Cl_2, each modeled with 50% occupancy values.

In the final cycles of refinement for **4** and **5**·4CH_2Cl_2, only atoms heavier than carbon were refined with anisotropic thermal parameters, owing to the large number of variables and the relatively weakly diffracting nature of the crystals; carbon atoms were refined with isotropic thermal parameters. For **7**·2CH_2Cl_2, the non-hydrogen atoms of the anion and cation were refined anisotropically, and those of the CH_2Cl_2 groups were refined isotropically. No hydrogen atoms were included. Final values of $R(F)$ and $R_w(F)$ are listed in Table 1.

Physical Measurements. Infrared spectra (Nujol mull) were recorded on a Nicolet Model 510P spectrophotometer (UV/vis). ^{1}H NMR spectra were recorded on a Varian XL-300D spectrometer with the protiosolvent signal used as a reference. Chemical shifts are quoted on the δ scale (downfield shifts are positive). EPR measurements were performed at X-band frequencies (9.4 GHz) on a Bruker ESP300 spectrometer with a Hewlett-Packard 5350B microwave frequency counter and an Oxford liquid He cryostat and temperature controller.

Variable-temperature magnetic susceptibility data for powdered samples of complexes **2** and **5**·CH_2Cl_2 (restrained in Parafilm to prevent torquing) were recorded in the temperature range 5−320 K and at an applied field of 10 kG on a SQUID susceptometer. Data were also collected in the temperature range 2−30 K at applied fields of 5−50 kG. A diamagnetic correction, estimated from Pascal's constants,[43] was subtracted from the experimental susceptibilities to give the molar paramagnetic susceptibilities.

Results

Syntheses. The preparation of $(NBu^n_4)[Mn_4O_2(O_2CPh)_9(H_2O)]$ (**4**) resulted from an investigation of the comproportionation reaction between $Mn(O_2CPh)_2{\cdot}2H_2O$ and $(NBu^n_4)[MnO_4]$ in EtOH/MeCN (2:1 v/v). The average Mn oxidation state in this reaction is 3.18, so the formation of a $4Mn^{III}$ product is not surprising. The isolated yields are almost quantitative (typically >85%) and the purity of the large red-black crystals is high, making this preparation a particularly convenient one. This complex is consequently an attractive starting point for further chemistry. As confirmed crystallographically (*vide infra*), complex **4** contains a $[Mn_4O_2]^{8+}$ butterfly unit essentially identical with those in previous examples of such complexes, but its peripheral ligation consists of only carboxylate and H_2O groups. As a result, it was anticipated that **4** would prove reactive toward a variety of reagents, including dicarboxylates, and this has proven to be the case.

The first task was to confirm that complex **4** maintains its structural integrity on dissolution in CH_2Cl_2; if it does not, it would be best considered a soluble source of manganese(III) benzoate rather than a convenient source of the $[Mn_4O_2]$ butterfly core. A Beer's law study in the concentration range 4.0−40 μM gave a linear dependence of absorbance on concentration, and **4** can be recovered unchanged by addition of hexanes to CH_2Cl_2 solutions. Together, these data are taken to indicate that the structure is maintained in this solvent. We have also shown elsewhere that **4** can be recovered unchanged from MeCN solutions.[28] More careful monitoring of solutions by, for example, NMR spectroscopy is precluded by the complexity of the spectrum.

The next question was whether simple ligand substitution reactions would occur with the chelating ligands bpy and pic$^-$ to give the known ions $[Mn_4O_2(O_2CPh)_7(bpy)_2]^+$ and $[Mn_4O_2(O_2CPh)_7(pic)_2]^-$, containing the chelate groups at wingtip positions. Treatment of **4** with 2 equiv of bpy did indeed give attachment of the bpy groups, but the product was identified as $Mn_4O_2(O_2CPh)_7(bpy)_2$ (**2**; $Mn^{II},3Mn^{III}$) rather than the expected $[Mn_4O_2(O_2CPh)_7(bpy)_2](O_2CPh)$ ($4Mn^{III}$); the source of the reducing equivalent is probably solvent, solvent impurities, or excess ligand groups, facilitated by the strongly oxidizing nature of Mn^{III}. It is interesting that the Et_2mal^{2-} product (*vide infra*) is also reduced *vis-à-vis* the starting complex **4**. The reaction (summarized in eq 1) is "all-or-nothing": addition of only 1

$$[Mn_4O_2(O_2CPh)_9(H_2O)]^- + 2bpy \xrightarrow{+e^-} Mn_4O_2(O_2CPh)_7(bpy)_2 + 2PhCO_2^- + H_2O \quad (1)$$

equiv of bpy leads to the same product but in lowered yield. Treatment of **4** with 2 equiv of picH or Na(pic) leads to an analogous reaction to give $(NBu^n_4)[Mn_4O_2(O_2CPh)_7(pic)_2]$ (**6**);

(43) *Theory and Applications of Molecular Paramagnetism*; Boudreaux, E. A.; Mulay, L. N., Eds.; J. Wiley & Sons: New York, 1976.

this time there is no metal reduction, the product being $4Mn^{III}$ (eq 2). Use of only 1 equiv of picH again gave a lowered yield of the bis chelate product, the precipitated solid being a mixture of **6** and **4**.

$$[Mn_4O_2(O_2CPh)_9(H_2O)]^- + 2picH \rightarrow [Mn_4O_2(O_2CPh)_7(pic)_2]^- + 2PhCO_2H + H_2O \quad (2)$$

Treatment of **4** with 2 equiv of dbmH did not give a bis chelate product, however. The product was $(NBu^n_4)[Mn_4O_2(O_2CPh)_8(dbm)]$ (**7**), whose crystal structure (*vide infra*) confirms an unusual and very asymmetric arrangement with a dbm^- group at only one wingtip position. This partial substitution at the wingtip sites is presumably a consequence of the poor donor properties of neutral dbmH and its low acidity ($pK_a = 13.4$)[44] hampering the overall displacement and protonation of the wingtip $PhCO_2^-$ group; the binding of the first dbm is presumably facilitated by the labile, terminally-bound H_2O group of **4**, whose dissociation could provide a binding site for neutral dbmH, which would lead to a lowering of its pK_a and trigger $PhCO_2^-$ displacement as $PhCO_2H$ (eq 3). If these arguments

$$[Mn_4O_2(O_2CPh)_9(H_2O)]^- + dbmH \rightarrow [Mn_4O_2(O_2CPh)_8(dbm)]^- + PhCO_2H + H_2O \quad (3)$$

are valid, then addition of the better donor dbm^- might lead to the displacement of the second wingtip $PhCO_2^-$ group and yield the bis chelate product. This was found to be the case; treatment of **7** with 1 equiv of Na(dbm) led to isolation of $(NBu^n_4)[Mn_4O_2(O_2CPh)_7(dbm)_2]$ (**8**). Complex **7** is the only mono chelate $[Mn_4O_2]^{8+}$ complex, and it may prove useful in the future for reactivity studies at the one available wingtip position. With the above experiments establishing the feasibility of clean ligand substitution reactions for complex **4**, attention now turned to the use of dicarboxylates.

As a potentially convenient route to $[Mn_4O_2]^{8+}$-containing complexes possessing dicarboxylate ligation, reactions were investigated between complex **4** and malonic acid derivatives in a 1:2 molar ratio. Preliminary experiments with malonic acid itself and with 2-monosubstituted derivatives led to a number of observations and problems that suggested the dicarboxylate might be susceptible to oxidation by **4**. Thus, efforts subsequently focused on more oxidation-resistant 2,2-disubstituted malonic acids, and the diethyl derivative was the one routinely employed. Treatment of complex **4** with 2 equiv of $Na_2(Et_2mal)$ in MeCN, followed by stirring of the slurry for *ca.* 1 week, leads to formation of a brown solution from which can be isolated a brown solid that can be recrystallized from CH_2Cl_2/hexanes to give $(NBu^n_4)_2[Mn_8O_4(O_2CPh)_{12}(Et_2mal)_2(H_2O)_2]\cdot 4CH_2Cl_2$ ($\mathbf{5}\cdot 4CH_2Cl_2$) in 45% overall yield. The formation of **5** is summarized in eq 4. Charge considerations necessitate a

$$2[Mn_4O_2(O_2CPh)_9(H_2O)]^- + 2Et_2mal^{2-} \xrightarrow{+2e^-} [Mn_8O_4(O_2CPh)_{12}(Et_2mal)_2(H_2O)_2]^{2-} + 6PhCO_2^- \quad (4)$$

$2Mn^{II},6Mn^{III}$ description for **5**, requiring the reduction of two Mn^{III} ions to have occurred, analogous to the formation of **2** ($Mn^{II},3Mn^{III}$) from the reaction of **4** with bpy; it is not uncommon to find Mn^{III}, a strong oxidizing agent, being reduced by ligand groups, solvent, solvent impurities, etc.[15] An alternative means for the generation of the Mn^{II} ions in **5** (and **2**) is disproportionation of Mn^{III}, in which case Mn^{IV}-containing species would be in the filtrate. We have not attempted to identify the exact origin of the Mn^{II} ions in **5**, nor would it be a simple matter to do so.

Table 2. Selected Fractional Coordinates ($\times 10^4$) and Equivalent[a] or Actual Isotropic Thermal Parameters ($Å^2$, $\times 10$) for $(NBu^n_4)[Mn_4O_2(O_2CPh)_9(H_2O)]$ (**4**)

atom	*x*	*y*	*z*	B_{eq}/B_{iso}
Mn(1)	2413(2)	2083(1)	2479(1)	23
Mn(2)	2584(2)	926(1)	3180(1)	21
Mn(3)	4077(2)	2042(1)	3462(1)	26
Mn(4)	840(1)	1774(1)	2954(1)	21
O(5)	3239(6)	1646(5)	2993(5)	22
O(6)	1745(6)	1482(5)	2775(4)	18
O(7)	3092(6)	2753(6)	2230(5)	23
O(8)	1560(6)	2387(6)	1892(5)	25
O(9)	2139(6)	2985(6)	2944(5)	24
O(10)	2605(7)	1257(6)	1920(5)	29
O(11)	2639(7)	1441(6)	3956(5)	28
O(12)	3427(7)	327(6)	3550(5)	25
O(13)	1828(6)	290(6)	3406(4)	22
O(14)	2626(7)	354(5)	2471(5)	24
O(15)	4389(6)	1084(6)	3893(5)	32
O(16)	3421(6)	2366(6)	3951(5)	26
O(17)	3966(7)	2984(6)	3016(5)	31
O(18)	4877(7)	1686(7)	3020(6)	45
O(19)	4928(7)	2466(6)	3965(5)	37
O(20)	917(6)	1057(6)	3553(5)	26
O(21)	495(6)	2331(6)	2261(5)	26
O(22)	−201(6)	1977(6)	3075(5)	26
O(23)	1276(7)	2607(6)	3414(5)	29
O(24)	−271(6)	1093(6)	2527(5)	25
O(25)	6029(8)	1997(9)	3854(7)	62
C(26)	3613(10)	3116(9)	2542(7)	29(4)
C(27)	840(10)	2464(9)	1880(7)	26(4)
C(28)	1789(10)	3033(9)	3309(7)	25(4)
C(29)	2693(10)	623(9)	2041(7)	21(3)
C(30)	2987(9)	1992(9)	4162(7)	21(3)
C(31)	4109(10)	487(9)	3839(8)	29(4)
C(32)	1384(10)	551(9)	3696(7)	28(4)
C(33)	−617(10)	1473(9)	2782(7)	22(4)
C(34)	5668(11)	2335(10)	4131(8)	35(4)
C(35)	3846(11)	3775(9)	2293(7)	28(4)
C(41)	345(10)	2716(9)	1352(7)	25(4)
C(47)	1956(10)	3678(9)	3666(7)	26(4)
C(53)	2927(10)	152(9)	1631(7)	26(4)
C(59)	2867(9)	2202(9)	4694(7)	22(3)
C(65)	4556(10)	−103(10)	4122(7)	28(4)
C(71)	1425(10)	233(9)	4232(7)	24(4)
C(77)	−1455(11)	1402(10)	2801(8)	34(4)
C(83)	6051(14)	2644(12)	4651(10)	52(5)

[a] $B_{eq} = {}^4/_3\sum\sum B_{ij}a_ia_j$.

The structure of **5** was shown by crystallography to contain an octanuclear core in which two $[Mn_4O_2]$ butterfly units have been linked together (*vide infra*). Although **5** is a new and interesting complex, the question that still arose was whether a discrete tetranuclear product might be attainable by suitable alteration of reaction conditions. A number of such attempts have been made, but without successful isolation of any other species; in particular, increasing the $Et_2mal:Mn_4$ reaction ratio still gives complex **5** as the isolable product. Complex **5** remains the only species to have been identified to date from the reaction of **4** with Et_2mal^{2-}.

Description of Structure. Selected fractional coordinates for **4**, $\mathbf{5}\cdot 4CH_2Cl_2$ and $\mathbf{7}\cdot 2CH_2Cl_2$, are listed in Tables 2−4, respectively; ORTEP representations are provided in Figures 1−4, and metric parameters are presented in Tables 5−7. The anions of **4** and $\mathbf{7}\cdot 2CH_2Cl_2$ lie on general positions whereas the anion of **5** lies on an inversion center, with the asymmetric unit thus containing half the anion. Complex $\mathbf{7}\cdot 2CH_2Cl_2$ contains two independent anions in the asymmetric unit. These are extremely similar structurally, and data for only one anion

(44) Olmstead, W. N.; Bardwell, F. G. *J. Org. Chem.* **1980**, *45*, 3295.

Table 3. Selected Fractional Coordinates ($\times 10^4$) and Equivalent[a] or Actual Isotropic Thermal Parameters (Å^2, $\times 10$) for $(NBu^n_4)_2[Mn_8O_4(O_2CPh)_{12}(Et_2mal)_2(H_2O)_2]$ (**5**)

atom	*x*	*y*	*z*	B_{eq}/B_{iso}
Mn(1)	278(1)	5555(1)	127(1)	18
Mn(2)	−157(1)	6003(1)	−1786(1)	22
Mn(3)	−1525(1)	5401(1)	−1046(1)	18
Mn(4)	−1257(1)	5280(1)	966(1)	19
O(5)	−461(6)	5693(3)	−989(6)	21
O(6)	−758(6)	5200(4)	42(6)	21
O(7)	−64(6)	6267(4)	547(6)	25
O(8)	164(6)	6298(4)	−2591(6)	26
C(9)	802(10)	6218(6)	−2813(10)	27(4)
O(10)	1098(11)	6541(5)	−3095(11)	79
C(11)	1166(11)	5702(6)	−2817(11)	34(4)
C(12)	1151(10)	5370(6)	−2143(10)	26(3)
O(13)	733(6)	5474(4)	−1664(6)	25
O(14)	1555(7)	4965(4)	−2016(6)	29
C(15)	2056(18)	5690(11)	−2831(18)	82(7)
C(16)	2710(19)	5862(11)	−2109(19)	89(8)
C(17)	355(17)	5429(11)	−3681(18)	81(7)
C(18)	178(25)	5699(16)	−4426(27)	136(12)
O(19)	1375(6)	5877(4)	192(6)	24
C(20)	1479(10)	6247(6)	−212(10)	26(3)
O(21)	921(6)	6397(4)	−877(7)	30
C(22)	2358(9)	6515(6)	179(10)	23(3)
C(23)	2954(12)	6413(7)	946(12)	43(5)
C(24)	3772(13)	6674(8)	1301(13)	52(5)
C(25)	3957(11)	7033(6)	860(11)	32(4)
C(26)	3382(14)	7140(8)	117(14)	56(5)
C(27)	2560(15)	6867(9)	−244(14)	60(6)
O(28)	−1181(6)	5570(4)	−2739(6)	29
C(29)	−1964(10)	5556(6)	−2807(10)	26(3)
O(30)	−2226(6)	5534(4)	−2215(6)	25
C(31)	−2727(10)	5544(6)	−3649(10)	27(3)
C(32)	−2516(11)	5557(6)	−4340(10)	32(4)
C(33)	−3220(10)	5526(6)	−5136(10)	31(4)
C(34)	−4082(11)	5503(7)	−5233(11)	38(4)
C(35)	−4319(12)	5484(7)	−4560(12)	41(4)
C(36)	−3614(11)	5517(6)	−3764(11)	33(4)
O(37)	−2143(6)	6018(3)	−708(6)	22
C(38)	−2245(9)	6124(5)	−54(9)	18(3)
O(39)	−1699(6)	6025(4)	672(6)	24
C(40)	−3068(10)	6417(6)	−183(10)	27(4)
C(41)	−3652(12)	6582(7)	−912(12)	39(4)
C(42)	−4435(14)	6831(8)	−1024(13)	53(5)
C(43)	−4614(16)	6914(9)	−369(17)	69(6)
C(44)	−4028(18)	6779(11)	430(18)	82(7)
C(45)	−3232(15)	6513(9)	513(15)	64(6)
O(46)	−2585(6)	5023(4)	−1132(6)	22
C(47)	−2913(10)	4951(6)	−598(11)	30(4)
O(48)	−2544(6)	5030(4)	165(6)	24
C(49)	−3860(13)	4746(8)	−948(13)	51(5)
C(50)	−4332(11)	4678(7)	−1785(11)	37(4)
C(51)	−5208(15)	4515(9)	−2082(15)	62(6)
C(52)	−5609(22)	4411(13)	−1562(23)	107(9)
C(53)	−5122(21)	4423(13)	−725(21)	100(9)
C(54)	−4193(15)	4576(9)	−380(15)	64(6)
O(55)	8(6)	5563(4)	1879(6)	23
C(56)	770(9)	5499(6)	1924(9)	21(3)
O(57)	970(6)	5372(4)	1316(6)	21
C(58)	1590(9)	5596(6)	2741(9)	21(3)
C(59)	1448(10)	5625(6)	3465(10)	25(3)
C(60)	2158(10)	5728(6)	4202(10)	30(4)
C(61)	2986(11)	5817(6)	4205(11)	34(4)
C(62)	3136(11)	5778(7)	3501(11)	36(4)
C(63)	2418(10)	5676(6)	2750(10)	25(4)
O(64)	−1086(6)	6502(4)	−1986(7)	27
C(65)	−1233(10)	6783(6)	−1463(10)	23(3)
O(66)	−716(7)	6856(4)	−746(7)	34
C(67)	−2097(10)	7067(6)	−1825(10)	28(4)
C(68)	−2769(13)	6954(7)	−2561(12)	45(5)
C(69)	−3577(15)	7234(9)	−2867(14)	60(6)
C(70)	−3644(15)	7603(9)	−2379(15)	63(6)
C(71)	−3003(14)	7721(8)	−1656(14)	51(5)
C(72)	−2239(12)	7438(7)	−1360(12)	41(4)

[a] $B_{eq} = {}^4/_3\sum\sum B_{ij}a_ia_j$.

Table 4. Selected[a] Fractional Coordinates ($\times 10^4$) and Equivalent[b] Isotropic Thermal Parameters (Å^2, $\times 10$) for $(NBu^n_4)[Mn_4O_2(O_2CPh)_8(dbm)]$ (**7**)

atom	*x*	*y*	*z*	B_{eq}
Mn(1)	2350(1)	2871(1)	329(1)	15
Mn(2)	755(1)	3761(1)	−114(1)	17
Mn(3)	2105(1)	4005(1)	966(1)	16
Mn(4)	3864(1)	3829(1)	739(1)	15
O(5)	1531(4)	3449(4)	409(3)	16
O(6)	2906(4)	3551(4)	772(3)	17
O(7)	1703(4)	2329(4)	−242(3)	19
C(8)	1345(6)	2608(6)	−653(5)	15
O(9)	967(4)	3153(4)	−679(3)	20
C(10)	1392(6)	2287(6)	−1206(5)	19
O(16)	2200(4)	2320(4)	1044(3)	20
C(17)	2178(6)	2620(6)	1498(5)	18
O(18)	2075(4)	3235(4)	1562(3)	19
C(19)	2221(6)	2154(7)	1983(5)	20
O(25)	3131(4)	2232(4)	272(3)	19
C(26)	3821(7)	2315(6)	265(4)	17
O(27)	4183(4)	2855(4)	430(3)	22
C(28)	4238(6)	1751(6)	51(4)	17
O(34)	2675(4)	3414(4)	−360(3)	19
C(35)	3115(6)	3874(6)	−398(5)	19
O(36)	3597(4)	4139(4)	−12(3)	18
C(37)	3094(7)	4183(6)	−956(4)	17
O(43)	−356(5)	3055(5)	−201(4)	29
C(44)	−596(7)	3461(6)	−574(5)	21
O(45)	−174(4)	3987(4)	−641(3)	19
C(46)	−1314(7)	3376(7)	−942(6)	28
O(52)	303(4)	4260(4)	443(3)	20
C(53)	547(7)	4410(6)	938(5)	20
O(54)	1201(4)	4383(4)	1198(3)	20
C(55)	−41(7)	4660(7)	1251(5)	23
O(61)	1275(4)	5603(4)	−390(3)	21
C(62)	1781(6)	4970(6)	−90(5)	16
O(63)	2019(4)	4891(4)	408(3)	19
C(64)	2066(6)	5561(6)	−357(6)	24
O(70)	2728(4)	4626(4)	1478(3)	19
C(71)	3266(6)	4995(6)	1388(5)	18
O(72)	3671(4)	4853(4)	1049(3)	20
C(73)	3437(6)	5606(6)	1708(5)	19
O(79)	4175(4)	3567(4)	1497(3)	17
C(80)	4812(7)	3360(6)	1727(5)	20
C(81)	5456(6)	3376(6)	1490(5)	20
C(82)	5456(6)	3705(6)	1005(5)	19
O(83)	4887(4)	4059(4)	732(3)	18
C(84)	4843(7)	3064(6)	2287(5)	21
C(90)	6099(7)	3664(6)	731(5)	22

[a] Selected coordinates are listed for only one of the two independent anions in the asymmetric unit; full listings for both anions are available in the Supporting Information. [b] $B_{eq} = {}^4/_3\sum\sum B_{ij}a_ia_j$.

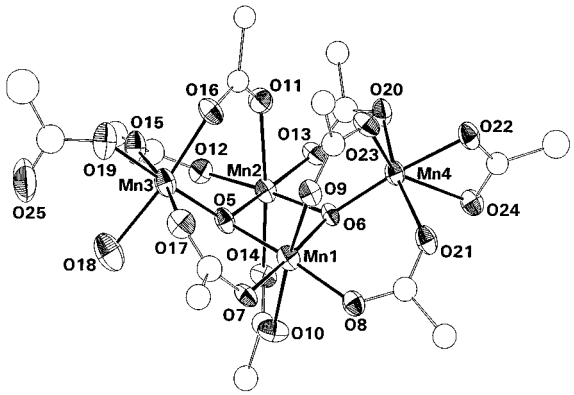

Figure 1. ORTEP representation of the $[Mn_4O_2(O_2CPh)_9(H_2O)]^-$ anion of complex **4** at the 50% probability level. For clarity, only one of the phenyl carbon atoms of the benzoate groups is shown.

are therefore presented. Full listings are available in the Supporting Information. The $NBu^n_4{}^+$ cations in the three structures will not be discussed.

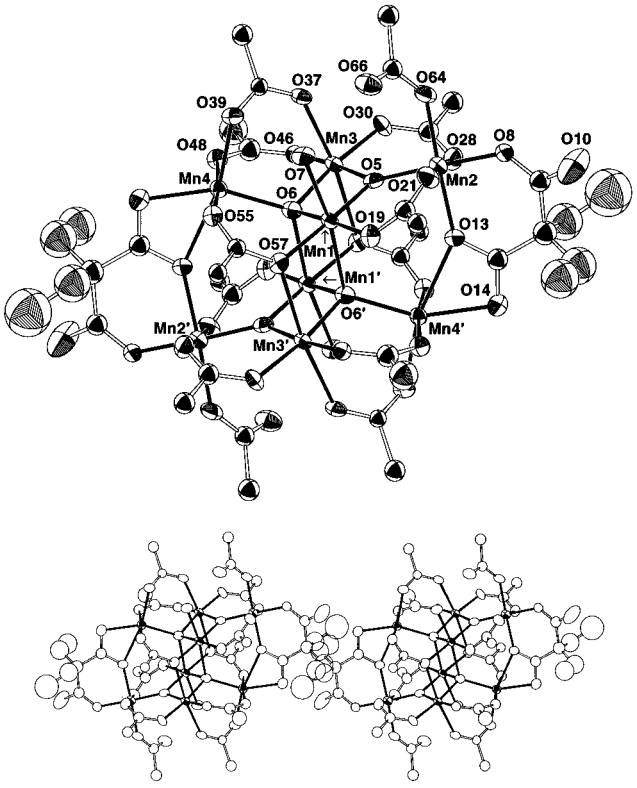

Figure 2. ORTEP representation and stereopair at the 50% probability level of the $[Mn_8O_4(O_2CPh)_{12}(Et_2mal)_2(H_2O)_2]^{2-}$ anion of **5**. For clarity, only one of the phenyl carbon atoms of the benzoate groups is shown. Primed and unprimed atoms are related by the crystallographic inversion center.

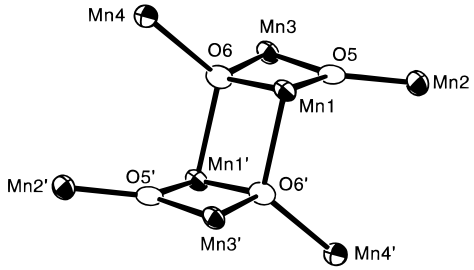

Figure 3. ORTEP representation of the $[Mn_8O_4]^{14+}$ core of the anion of **5**, emphasizing the linked-butterfly structure and the coordination number and geometry of the oxygen atoms.

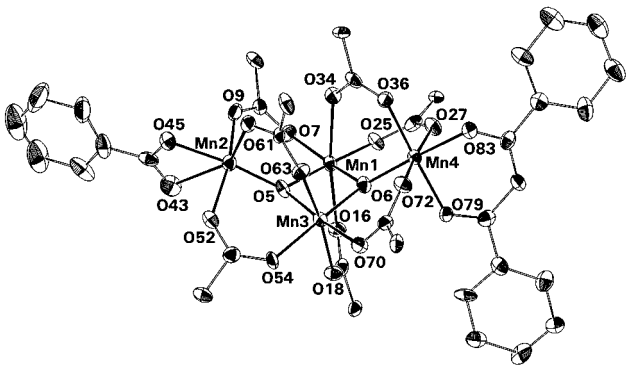

Figure 4. ORTEP representation of the $[Mn_4O_2(O_2CPh)_8(dbm)]^-$ anion of **7** at the 50% probability level. For clarity, only one of the phenyl carbon atoms of the *bridging* benzoate groups is shown.

The anion of complex **4** has a butterfly $[Mn_4O_2]^{8+}$ core ($4Mn^{III}$) similar to those in, for example, $[Mn_4O_2(O_2CMe)_7(bpy)_2](ClO_4)$ (**3**; R = Me) and $(NBu^n_4)[Mn_4O_2(O_2CMe)_7(pic)_2]$ (**6**).[15,16] The dihedral angle between the two Mn_3 planes is 131.0° and it has two types of Mn···Mn separations, with values of 2.816 Å for Mn(1)···Mn(2) and 3.302−3.367 Å for the others. These values are similar to those for the bpy and pic^- complexes. However, the absence of chelating bpy or pic^- groups has some consequences: Mn(4) possesses an additional benzoate group in a rare asymmetric chelating mode, with Mn(4)−O(24) (2.373(11) Å) being much longer than Mn(4)−O(22) (1.947(11) Å). Thus, Mn(4) has a very distorted octahedral coordination environment with O(22)−Mn(4)−O(24) being only 59.6(4)°. There is also an additional benzoate group at Mn(3), but this is ligated in a monodentate fashion; the remaining site is occupied by a terminal H_2O molecule (O(18)), and the latter is strongly hydrogen-bonded to the unligated benzoate oxygen atom O(25), with an O(18)···O(25) distance of 2.634(24) Å.

The anion of complex **5** consists of an $[Mn_8(\mu_4\text{-}O)_2(\mu_3\text{-}O)_2]$ core with peripheral ligation provided by two terminal and ten bridging $PhCO_2^-$ groups, two terminal water molecules (O(7) and O(7′)) on Mn(1) and Mn(1′), and two bridging Et_2mal^{2-} groups. The uncoordinated O atoms of the monodentate

Table 5. Selected Interatomic Distances (Å) and Angles (deg) for $(NBu^n_4)[Mn_4O_2(O_2CPh)_9(H_2O)]$ (**4**)

Mn(1)···Mn(2)	2.816(4)	Mn(2)···Mn(3)	3.302(4)
Mn(1)···Mn(3)	3.367(4)	Mn(2)···Mn(4)	3.365(4)
Mn(1)···Mn(4)	3.296(4)	O(18)···O(25)	2.634(24)
Mn(1)−O(5)	1.900(11)	Mn(3)−O(5)	1.823(11)
Mn(1)−O(6)	1.909(10)	Mn(3)−O(15)	2.136(12)
Mn(1)−O(7)	1.946(11)	Mn(3)−O(16)	1.982(11)
Mn(1)−O(8)	1.940(12)	Mn(3)−O(17)	2.111(12)
Mn(1)−O(9)	2.206(11)	Mn(3)−O(18)	2.102(13)
Mn(1)−O(10)	2.206(12)	Mn(3)−O(19)	1.903(13)
Mn(2)−O(5)	1.913(10)	Mn(4)−O(6)	1.825(10)
Mn(2)−O(6)	1.905(11)	Mn(4)−O(20)	2.038(12)
Mn(2)−O(11)	2.202(12)	Mn(4)−O(21)	2.037(12)
Mn(2)−O(12)	1.923(11)	Mn(4)−O(22)	1.947(11)
Mn(2)−O(13)	1.973(11)	Mn(4)−O(23)	2.016(12)
Mn(2)−O(14)	2.136(11)	Mn(4)−O(24)	2.373(11)

O(15)−Mn(3)−O(19)	87.0(5)	O(6)−Mn(1)−O(7)	174.9(5)
O(16)−Mn(3)−O(17)	94.9(5)	O(6)−Mn(1)−O(8)	93.5(5)
O(16)−Mn(3)−O(18)	173.5(5)	O(6)−Mn(1)−O(9)	91.3(4)
O(16)−Mn(3)−O(19)	84.8(5)	O(6)−Mn(1)−O(10)	91.8(4)
O(17)−Mn(3)−O(18)	88.3(5)	O(7)−Mn(1)−O(8)	87.8(5)
O(17)−Mn(3)−O(19)	88.0(5)	O(7)−Mn(1)−O(9)	83.8(4)
O(18)−Mn(3)−O(19)	89.7(6)	O(7)−Mn(1)−O(10)	93.3(4)
O(6)−Mn(4)−O(20)	94.5(5)	O(8)−Mn(1)−O(9)	88.0(4)
O(6)−Mn(4)−O(21)	92.0(5)	O(8)−Mn(1)−O(10)	85.0(5)
O(6)−Mn(4)−O(22)	171.6(5)	O(9)−Mn(1)−O(10)	172.5(4)
O(6)−Mn(4)−O(23)	99.1(5)	O(5)−Mn(2)−O(6)	83.7(4)
O(6)−Mn(4)−O(24)	112.0(4)	O(5)−Mn(2)−O(11)	90.3(5)
O(20)−Mn(4)−O(21)	164.1(5)	O(5)−Mn(2)−O(12)	96.8(5)
O(20)−Mn(4)−O(22)	84.9(5)	O(5)−Mn(2)−O(13)	172.1(5)
O(20)−Mn(4)−O(23)	97.8(5)	O(5)−Mn(2)−O(14)	90.6(5)
O(20)−Mn(4)−O(24)	83.4(4)	O(6)−Mn(2)−O(11)	96.4(4)
O(21)−Mn(4)−O(22)	86.6(5)	O(6)−Mn(2)−O(12)	176.3(5)
O(21)−Mn(4)−O(23)	95.5(5)	O(6)−Mn(2)−O(13)	91.3(4)
O(21)−Mn(4)−O(24)	80.7(4)	O(6)−Mn(2)−O(14)	89.6(5)
O(22)−Mn(4)−O(23)	89.3(5)	O(11)−Mn(2)−O(12)	87.2(5)
O(22)−Mn(4)−O(24)	59.6(4)	O(11)−Mn(2)−O(13)	84.2(4)
O(23)−Mn(4)−O(24)	148.7(4)	O(11)−Mn(2)−O(14)	174.0(4)
Mn(1)−O(5)−Mn(2)	95.2(5)	O(12)−Mn(2)−O(13)	88.5(5)
Mn(1)−O(5)−Mn(3)	129.4(6)	O(12)−Mn(2)−O(14)	86.8(5)
Mn(2)−O(5)−Mn(3)	124.2(6)	O(13)−Mn(2)−O(14)	95.4(4)
Mn(1)−O(6)−Mn(2)	95.2(4)	O(5)−Mn(3)−O(15)	93.2(5)
Mn(1)−O(6)−Mn(4)	123.9(6)	O(5)−Mn(3)−O(16)	93.2(5)
Mn(2)−O(6)−Mn(4)	128.9(6)	O(5)−Mn(3)−O(17)	92.1(5)
O(5)−Mn(1)−O(6)	83.9(5)	O(5)−Mn(3)−O(18)	92.3(5)
O(5)−Mn(1)−O(7)	95.6(5)	O(5)−Mn(3)−O(19)	178.0(5)
O(5)−Mn(1)−O(8)	170.8(5)	O(15)−Mn(3)−O(16)	92.9(5)
O(5)−Mn(1)−O(9)	100.9(4)	O(15)−Mn(3)−O(17)	170.3(4)
O(5)−Mn(1)−O(10)	86.3(5)	O(15)−Mn(3)−O(18)	83.4(5)

Table 6. Selected Interatomic Distances (Å) and Angles (deg) for $(NBu^n_4)[Mn_8O_4(O_2CPh)_{12}(Et_2mal)_2(H_2O)_2]$ (**5**)

Mn(1)···Mn(1′)	3.128(3)	Mn(2)−O(13)	1.988(9)
Mn(1)···Mn(2)	3.396(4)	Mn(2)−O(21)	2.126(11)
Mn(1)···Mn(3)	2.851(4)	Mn(2)−O(28)	2.173(11)
Mn(1)···Mn(3′)	3.290(4)	Mn(2)−O(64)	1.951(10)
Mn(1)···Mn(4)	3.463(3)	Mn(3)−O(5)	1.867(9)
Mn(1)···Mn(4′)	3.733(3)	Mn(3)−O(6)	1.902(10)
Mn(2)···Mn(3)	3.420(3)	Mn(3)−O(30)	1.949(10)
Mn(2)···Mn(4′)	4.105(4)	Mn(3)−O(37)	2.162(10)
Mn(3)···Mn(4)	3.427(4)	Mn(3)−O(46)	1.958(10)
Mn(1)−O(5)	1.888(10)	Mn(3)−O(57′)	2.408(10)
Mn(1)−O(6)	1.891(10)	Mn(4)−O(6)	2.113(10)
Mn(1)−O(6′)	2.258(10)	Mn(4)−O(13′)	2.367(10)
Mn(1)−O(7)	2.224(10)	Mn(4)−O(14′)	2.207(10)
Mn(1)−O(19)	1.948(10)	Mn(4)−O(39)	2.141(10)
Mn(1)−O(57)	2.006(10)	Mn(4)−O(48)	2.106(10)
Mn(2)−O(5)	1.874(10)	Mn(4)−O(55)	2.176(9)
Mn(2)−O(8)	1.885(10)		

O(5)−Mn(1)−O(6)	81.4(4)	O(6)−Mn(3)−O(37)	97.4(4)
O(5)−Mn(1)−O(6′)	98.5(4)	O(6)−Mn(3)−O(46)	97.0(4)
O(5)−Mn(1)−O(7)	92.2(4)	O(6)−Mn(3)−O(57′)	78.9(4)
O(5)−Mn(1)−O(19)	98.6(4)	O(30)−Mn(3)−O(37)	90.7(4)
O(5)−Mn(1)−O(57)	174.8(4)	O(30)−Mn(3)−O(46)	84.2(4)
O(6)−Mn(1)−O(6′)	82.5(4)	O(30)−Mn(3)−O(57′)	93.2(4)
O(6)−Mn(1)−O(7)	97.8(4)	O(37)−Mn(3)−O(46)	86.3(4)
O(6′)−Mn(1)−O(7)	169.2(4)	O(37)−Mn(3)−O(57′)	170.2(3)
O(6)−Mn(1)−O(19)	175.9(4)	O(46)−Mn(3)−O(57′)	85.1(4)
O(6′)−Mn(1)−O(19)	93.4(4)	O(6)−Mn(4)−O(13′)	98.4(4)
O(6)−Mn(1)−O(57)	93.4(4)	O(6)−Mn(4)−O(14′)	155.1(4)
O(6′)−Mn(1)−O(57)	80.6(4)	O(6)−Mn(4)−O(39)	96.0(4)
O(7)−Mn(1)−O(19)	86.3(4)	O(6)−Mn(4)−O(48)	91.9(4)
O(7)−Mn(1)−O(57)	88.6(4)	O(6)−Mn(4)−O(55)	93.9(4)
O(19)−Mn(1)−O(57)	86.6(4)	O(13′)−Mn(4)−O(14′)	56.9(4)
O(5)−Mn(2)−O(8)	178.3(4)	O(13′)−Mn(4)−O(39)	163.8(4)
O(5)−Mn(2)−O(13)	89.7(4)	O(13′)−Mn(4)−O(48)	97.0(4)
O(5)−Mn(2)−O(21)	92.5(4)	O(13′)−Mn(4)−O(55)	83.5(4)
O(5)−Mn(2)−O(28)	89.4(4)	O(14′)−Mn(4)−O(39)	108.9(4)
O(5)−Mn(2)−O(64)	91.7(4)	O(14′)−Mn(4)−O(48)	88.5(4)
O(8)−Mn(2)−O(13)	88.7(4)	O(14′)−Mn(4)−O(55)	86.8(4)
O(8)−Mn(2)−O(21)	87.9(4)	O(48)−Mn(4)−O(55)	174.0(4)
O(8)−Mn(2)−O(28)	90.1(4)	O(39)−Mn(4)−O(48)	89.9(4)
O(8)−Mn(2)−O(64)	89.9(4)	O(39)−Mn(4)−O(55)	88.2(4)
O(13)−Mn(2)−O(21)	86.7(4)	Mn(1)−O(5)−Mn(2)	129.0(5)
O(13)−Mn(2)−O(28)	89.2(4)	Mn(1)−O(5)−Mn(3)	98.8(5)
O(13)−Mn(2)−O(64)	175.7(5)	Mn(2)−O(5)−Mn(3)	132.2(5)
O(21)−Mn(2)−O(28)	175.4(4)	Mn(1)−O(6)−Mn(1′)	97.5(4)
O(21)−Mn(2)−O(64)	97.3(4)	Mn(1′)−O(6)−Mn(3)	104.2(4)
O(28)−Mn(2)−O(64)	86.8(4)	Mn(1)−O(6)−Mn(3)	97.5(5)
O(5)−Mn(3)−O(6)	81.7(4)	Mn(1′)−O(6)−Mn(4)	117.3(4)
O(5)−Mn(3)−O(30)	96.2(4)	Mn(1)−O(6)−Mn(4)	119.6(5)
O(5)−Mn(3)−O(37)	100.3(4)	Mn(3)−O(6)−Mn(4)	117.2(4)
O(5)−Mn(3)−O(46)	173.3(4)	Mn(2)−O(13)−Mn(4′)	117.2(4)
O(5)−Mn(3)−O(57′)	88.2(4)	Mn(1)−O(57)−Mn(3′)	95.9(4)
O(6)−Mn(3)−O(30)	171.8(4)		

$PhCO_2^-$ groups (O(66) and O(66′)) are hydrogen-bonded to the H_2O molecules (O(66)···O(7) = 2.639(18) Å). The $[Mn_8O_4]$ core may be conveniently described as two $[Mn_4O_2]$ butterfly units [atoms Mn(1)−Mn(4) and their symmetry-related partners] becoming linked by one μ_3-O^{2-} ion in each unit converting to a μ_4 mode and thus providing the two interbutterfly bonds, Mn(1)−O(6′) and Mn(1′)−O(6). The $[Mn_8O_4]$ core alone is shown in Figure 3; as can be clearly seen, the coordination geometry at O(6) is distorted tetrahedral while that at O(5) is essentially trigonal planar. As a result of the linkage, each $[Mn_4O_2]$ butterly unit has become "flattened" relative to that in the parent $[Mn_4O_2(PhCO_2)_9(H_2O)]^-$ anion of **4**; the dihedral angles of the Mn_4 butterflies in **5** and **4** are 162.2 and 131.0°, respectively.

Charge considerations require a $2Mn^{II},6Mn^{III}$ oxidation state description, and the Mn^{II} ions are assigned as Mn(4) and Mn(4′) on the basis of (i) the longer average Mn−O bond lengths at these ions (average 2.185 Å and no individual value shorter than 2.1 Å) compared with those for the other Mn ions (average 2.000−2.041 Å) and (ii) the clear presence of a Jahn−Teller (JT) axial elongation at Mn(1), Mn(2), and Mn(3), as expected for a high-spin d^4 ion in near-octahedral geometry. Thus, axially-elongated bonds are longer than equatorial bonds by at least 0.15 Å. The JT elongation axes at Mn(1) (O(7)−Mn(1)−O(6′)) and Mn(3) (O(37)−Mn(3)−O(57′)) are nearly coplanar with the central $[Mn_2O_2]$ rhombus whereas the JT axis at Mn2 (O21-Mn(2)−O(28)) is nearly perpendicular. A major consequence of this positioning of the JT axes is that the two interbutterfly linkages, Mn(1)−O(6′) and Mn(1′)−O(6) are on JT elongation axes. As a result, they are the longest Mn−O^{2-} bonds in the molecule (2.258(10) Å), even longer than the Mn^{II}−O^{2-} bond, Mn(4)−O(6) = 2.113(10) Å; on an absolute scale, these are remarkably long distances for an Mn^{III}−O^{2-} bond, whose typical value is ∼1.9 Å, even when the O^{2-} ion is μ_4.[45] The possible influence of these long Mn^{III}−O^{2-} bonds on the magnetic properties of **5** will be discussed below (*vide infra*).

Table 7. Selected Interatomic Distances (Å) and Angles (deg) for $(NBu^n_4)[Mn_4O_2(O_2CPh)_8(dbm)]$ (**7**)[a]

Mn(1)−Mn(2)	3.379(3)	Mn(2)−O(52)	2.011(8)
Mn(1)−Mn(3)	2.828(3)	Mn(2)−O(61)	2.093(8)
Mn(1)−Mn(4)	3.325(3)	Mn(3)−O(5)	1.909(8)
Mn(2)−Mn(3)	3.304(3)	Mn(3)−O(6)	1.853(8)
Mn(3)−Mn(4)	3.374(2)	Mn(3)−O(18)	2.135(8)
Mn(1)−O(5)	1.915(7)	Mn(3)−O(54)	1.992(8)
Mn(1)−O(6)	1.897(8)	Mn(3)−O(63)	2.219(8)
Mn(1)−O(7)	1.973(8)	Mn(3)−O(70)	1.960(8)
Mn(1)−O(16)	2.157(8)	Mn(4)−O(6)	1.842(7)
Mn(1)−O(25)	1.924(8)	Mn(4)−O(27)	2.188(8)
Mn(1)−O(34)	2.207(8)	Mn(4)−O(36)	1.944(8)
Mn(2)−O(5)	1.830(8)	Mn(4)−O(72)	2.211(8)
Mn(2)−O(9)	1.948(8)	Mn(4)−O(79)	1.938(8)
Mn(2)−O(43)	2.423(9)	Mn(4)−O(83)	1.915(8)
Mn(2)−O(45)	1.974(8)		

O(5)−Mn(1)−O(6)	81.6(3)	O(5)−Mn(3)−O(6)	82.9(3)
O(5)−Mn(1)−O(7)	92.0(3)	O(5)−Mn(3)−O(18)	91.0(3)
O(5)−Mn(1)−O(16)	88.9(3)	O(5)−Mn(3)−O(54)	93.7(3)
O(5)−Mn(1)−O(25)	175.3(3)	O(5)−Mn(3)−O(63)	91.8(3)
O(5)−Mn(1)−O(34)	97.5(3)	O(5)−Mn(3)−O(70)	174.3(3)
O(6)−Mn(1)−O(7)	167.6(3)	O(6)−Mn(3)−O(18)	88.4(3)
O(6)−Mn(1)−O(16)	90.5(3)	O(6)−Mn(3)−O(54)	173.1(4)
O(6)−Mn(1)−O(25)	100.9(3)	O(6)−Mn(3)−O(63)	100.1(3)
O(6)−Mn(1)−O(34)	85.5(3)	O(6)−Mn(3)−O(70)	95.1(3)
O(7)−Mn(1)−O(16)	100.0(3)	O(18)−Mn(3)−O(54)	85.6(3)
O(7)−Mn(1)−O(25)	86.2(3)	O(18)−Mn(3)−O(63)	171.4(3)
O(7)−Mn(1)−O(34)	84.8(3)	O(18)−Mn(3)−O(70)	94.4(3)
O(16)−Mn(1)−O(25)	87.1(3)	O(54)−Mn(3)−O(63)	86.1(3)
O(16)−Mn(1)−O(34)	171.9(3)	O(54)−Mn(3)−O(70)	88.8(3)
O(25)−Mn(1)−O(34)	86.7(3)	O(63)−Mn(3)−O(70)	83.2(3)
O(5)−Mn(2)−O(9)	94.5(3)	O(6)−Mn(4)−O(27)	94.3(3)
O(5)−Mn(2)−O(43)	112.4(3)	O(6)−Mn(4)−O(36)	94.6(3)
O(5)−Mn(2)−O(45)	171.2(3)	O(6)−Mn(4)−O(72)	92.1(3)
O(5)−Mn(2)−O(52)	91.7(3)	O(6)−Mn(4)−O(79)	88.3(3)
O(5)−Mn(2)−O(61)	99.7(3)	O(6)−Mn(4)−O(83)	175.8(3)
O(9)−Mn(2)−O(43)	82.3(3)	O(27)−Mn(4)−O(36)	88.1(3)
O(9)−Mn(2)−O(45)	85.5(3)	O(27)−Mn(4)−O(72)	173.6(3)
O(9)−Mn(2)−O(52)	166.1(3)	O(27)−Mn(4)−O(79)	93.9(3)
O(9)−Mn(2)−O(61)	94.5(3)	O(27)−Mn(4)−O(83)	83.0(3)
O(43)−Mn(2)−O(45)	58.9(3)	O(36)−Mn(4)−O(72)	91.5(3)
O(43)−Mn(2)−O(52)	83.9(3)	O(36)−Mn(4)−O(79)	176.4(3)
O(43)−Mn(2)−O(61)	147.9(3)	O(36)−Mn(4)−O(83)	88.5(3)
O(45)−Mn(2)−O(52)	86.6(3)	O(72)−Mn(4)−O(79)	86.2(3)
O(45)−Mn(2)−O(61)	89.1(3)	O(72)−Mn(4)−O(83)	90.6(3)
O(52)−Mn(2)−O(61)	96.7(3)	O(79)−Mn(4)−O(83)	88.7(3)

[a] Only for one of the two independent anions in the asymmetric unit; full listings are available in the Supporting Information.

(45) Halcrow, M. A.; Streib, W. E.; Folting, K.; Christou, G. *Acta Crystallogr., Sect. C* **1995**, *C51*, 1263.

The two Et_2mal^{2-} groups are in an unusual and asymmetric ligation mode:

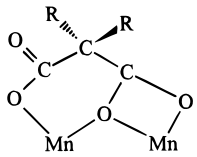

The Et_2mal^{2-} group thus forms a four-membered chelate ring at Mn(4) and a six-membered chelate ring at Mn(2′), with one O atom, O(13), monoatomically bridging the two metals. Since the latter are in different halves of the linked-butterfly assembly, the two Et_2mal groups are bridging the two butterfly units, and this no doubt contributes to the formation and stabilization of an octanuclear product.

Malonates have been observed in numerous ligation modes over the years,[46] but the particular asymmetric mode observed in **5** is unprecedented, although it is related to one of the symmetric modes present in $Eu_2(mal)_3 \cdot 8H_2O$, shown as follows for comparison:[47]

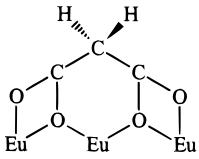

The anion of complex **7** is very similar to that in **4**, except that the monodentate $PhCO_2^-$ and H_2O groups at one wingtip position of the $[Mn_4O_2]^{8+}$ butterfly unit have been replaced by a chelating dbm^- group. The other wingtip position retains a chelating $PhCO_2^-$ group. The distances and angles in the two complexes are very similar. It is interesting to note also the similarity between the structures of **7** and **5**: in both complexes, the $[Mn_4O_2]$ butterfly units have a six-membered chelate ring (dbm^- (**7**) or Et_2mal^{2-} (**5**)) at one wingtip position and a four-membered chelate ring ($PhCO_2^-$ (**7**) or one Et_2mal^{2-} carboxylate (**5**)) at the other. The dual ability of a *single* Et_2mal^{2-} group to provide *both* types of chelate rings is undoubtedly one of the contributing factors in yielding the octanuclear, "linked-butterfly" structure for **5**.

Magnetochemistry Studies

A variable-temperature magnetic susceptibility study was performed on polycrystalline samples of $Mn_4O_2(O_2CPh)_7(bpy)_2$ (**2**) and $(NBu^n_4)_2[Mn_8O_4(O_2CPh)_{12}(Et_2mal)_2(H_2O)_2]$ (**5**), restrained in Parafilm to prevent torquing. The magnetic susceptibility of both complexes was examined in a 10.0 kG field in the 5.0−320.0 K temperature range. The effective magnetic moment (μ_{eff}) of complex **2** gradually decreases from 8.61 μ_B per molecule at 320.0 K to 5.71 μ_B at 13.0 K and then slightly increases to 5.91 μ_B at 5.0 K (Figure 5). The slight increase observed at low temperatures is most likely due to a small amount of a paramagnetic impurity. The effective magnetic moment of 8.61 μ_B per molecule is less than the 10.34 μ_B spin-only value ($g = 2.0$) expected for a $Mn^{II}Mn^{III}_3$ complex with noninteracting metal centers. Similarly, the effective magnetic moment of **5** gradually decreases from 10.54 μ_B per molecule at 320.0 K to 8.42 μ_B at 40.0 K, followed by a more rapid decrease to 6.02 μ_B at 5.0 K (Figure 6). The effective magnetic moment of 10.54 μ_B per molecule at 320 K is less than the 14.63 μ_B spin-only value ($g = 2.0$) expected for a $Mn^{II}_2Mn^{III}_6$ complex with noninteracting metal centers. For both complexes, the effective magnetic moment being less than the spin-only value suggests the presence of net antiferromagnetic interactions within the manganese−oxide cores.

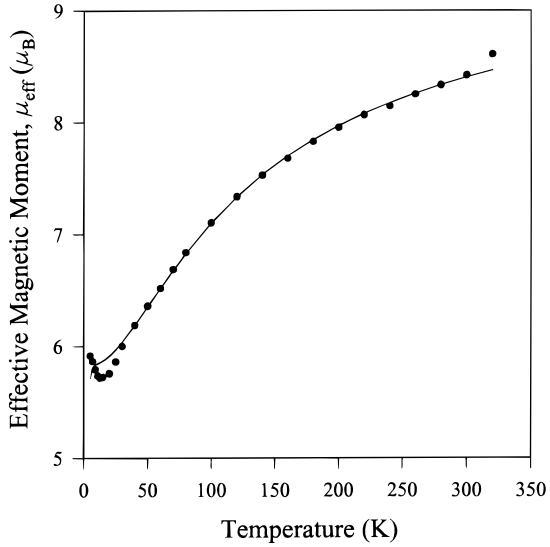

Figure 5. Plot of effective magnetic moment (μ_{eff} per Mn_4) *vs* temperature for $[Mn_4O_2(O_2CPh)_7(bpy)_2]$ (**2**). The solid line is a fit of the data to the appropriate theoretical expression; see text for fitting parameters.

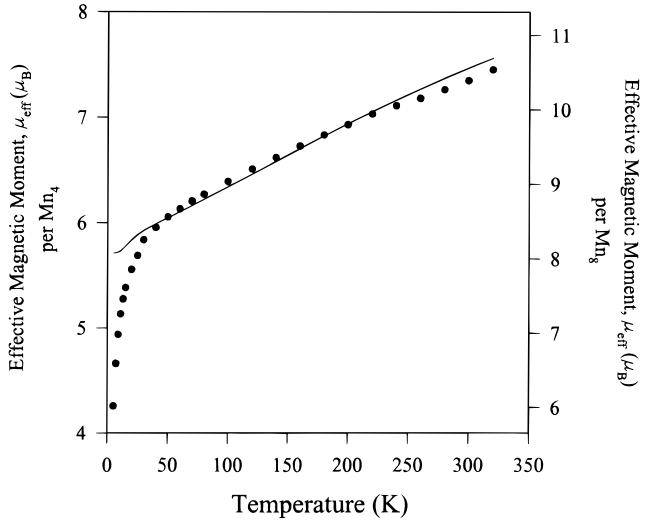

Figure 6. Plot of effective magnetic moment (μ_{eff}) per Mn_4 (left axis) and per Mn_8 (right axis) *vs* temperature for $(NBu^n_4)_2[Mn_8O_4(O_2CPh)_{12}(Et_2mal)_2(H_2O)_2]$ (**5**). The solid line is a fit of the data for temperatures ≥40 K to the appropriate theoretical expression; see text for fitting parameters.

$Mn_4O_2(O_2CPh)_7(bpy)_2$ (2). We shall first address the fitting of the data for complex **2**. As discussed in the previous section, the X-ray structural characterization of **2** has not been accomplished but the structure of **5**, containing two of the same $[Mn^{II}Mn^{III}_3O_2]^{7+}$ butterfly units as present in **2**, strongly supports the conclusion that the Mn^{II} ion in **2** is at a wingtip position. The $[Mn_4O_2]^{7+}$ core of **2** thus has idealized C_s symmetry, requiring three parameters (J) to describe the magnetic exchange interactions between the four metal centers (Scheme 1); a fourth exchange parameter J_{ww}, describing the interaction between

(46) Representative manganese complexes: (a) Lis, T.; Matuszewski, J.; Jeźowska-Trzebiatowska, B. *Acta Crystallogr., Sect. B* **1977**, *33*, 1943. (b) Lis, T.; Matuszewski, J. *Acta Crystallogr., Sect. B* **1979**, *35*, 2212. (c) Lis, T.; Matuszewski, J. *J. Chem. Soc., Dalton Trans.* **1980**, 996. (d) Saadeh, S. M.; Trojan, K. L.; Kampf, J. W.; Hatfield, W. E.; Pecoraro, V. L. *Inorg. Chem.* **1993**, *32*, 3034. (e) Haselhorst, G.; Wieghardt, K. *J. Inorg. Biochem.* **1995**, *59*, 624.

(47) Hansson, E. *Acta Chem. Scand.* **1973**, *27*, 2827.

Scheme 1

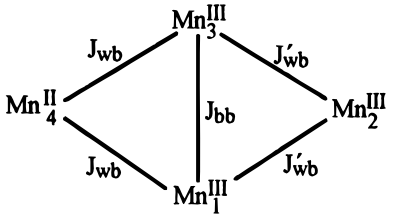

the two wingtip Mn atoms, is taken as zero, as is customary for such butterfly complexes given the large distance between these metal atoms.[15] The Heisenberg spin Hamiltonian that describes the possible pairwise interactions in Scheme 1 is given by eq 5, where $\hat{S}_i$ represents the spin operator for metal Mn_i. A

$$\hat{H} = -2J_{bb}\hat{S}_1\cdot\hat{S}_3 - 2J_{wb}(\hat{S}_1\cdot\hat{S}_4 + \hat{S}_3\cdot\hat{S}_4) - 2J_{wb}'(\hat{S}_1\cdot\hat{S}_2 + \hat{S}_2\cdot\hat{S}_3) \quad (5)$$

full-matrix diagonalization approach for obtaining the eigenvalues of this spin Hamiltonian would require diagonalization of a 750 × 750 matrix. Unfortunately, the more convenient equivalent operator approach, based on the Kambe vector coupling method,[49] is not possible for the C_s symmetry system of Scheme 1. Thus, a simplifying approximation was introduced, namely that all exchange interactions between wingtip and body Mn atoms are equivalent; i.e. $J_{wb} = J'_{wb}$. This is a reasonable approximation, in fact, because exchange interactions between Mn atoms in [Mn^{III}(μ_3-O)Mn^{III}] and [Mn^{II}(μ_3-O)Mn^{III}] units are known to be of comparable magnitude, −2.7 to −10.2 and −1.5 to −6.5 cm^{-1}, respectively (Table 8). With this approximation, the spin Hamiltonian of eq 5 simplifies to that in eq 6, which is the same as that employed to analyze the

$$\hat{H} = -2J_{bb}(\hat{S}_1\cdot\hat{S}_3) - 2J_{wb}(\hat{S}_1\cdot\hat{S}_2 + \hat{S}_1\cdot\hat{S}_4 + \hat{S}_2\cdot\hat{S}_3 + \hat{S}_3\cdot\hat{S}_4) \quad (6)$$

magnetic interactions within the $[Mn_4O_2]^{6+,8+}$ cores of the other tetranuclear complexes in Table 8, with $2Mn^{II}$,$2Mn^{III}$ or $4Mn^{III}$ oxidation states and idealized C_{2v} core symmetry. In the present case, however, $S_1 = S_2 = S_3 = 2$ and $S_4 = {}^5/_2$. The Kambe vector coupling method can now be employed,[49] with the following coupling scheme:

$$\hat{S}_{13} = \hat{S}_1 + \hat{S}_3; \quad \hat{S}_{24} = \hat{S}_2 + \hat{S}_4; \quad \hat{S}_T = \hat{S}_{13} + \hat{S}_{24}$$

where S_T is the total spin of the Mn_4 complex. The spin Hamiltonian of eq 6 can now be expressed in the equivalent form of eq 7, and the energies (E) of the spin states (S_T) are

$$\hat{H} = -J_{wb}(\hat{S}_T^{\,2} - \hat{S}_{13}^{\,2} - \hat{S}_{24}^{\,2}) - J_{bb}(\hat{S}_{13}^{\,2} - \hat{S}_1^{\,2} - \hat{S}_3^{\,2}) \quad (7)$$

given by eq 8, where constant terms have been ignored. The

$$E = -J_{wb}[S_T(S_T+1) - S_{13}(S_{13}+1) - S_{24}(S_{24}+1)] - J_{bb}[S_{13}(S_{13}+1)] \quad (8)$$

overall degeneracy of this spin system is 750, made up of 95 individual spin states ranging from $S_T = {}^1/_2$ to ${}^{17}/_2$.

A theoretical expression for the molar paramagnetic susceptibility (χ_m) *versus* temperature was derived for complex **2** by using the Van Vleck equation and assuming an isotropic g value. This expression was employed to fit the experimental χ_m *vs* T data, and the parameters varied were J_{wb}, J_{bb}, and g; a temperature-independent paramagnetism (TIP) term was held constant at 800×10^{-6} cm^3 mol^{-1}. Only data for temperatures ≥40 K were employed in the fit to avoid complications at low temperature from zero-field splitting of $S_T \geq {}^3/_2$ terms and the tail in the data that is indicative of a small amount of paramagnetic impurity, and to make the data analysis for **2** more comparable with that for **5** (*vide infra*) where only data for $T \geq 40$ K were employed. The fit parameters were $J_{bb} = -9.2$ cm^{-1}, $J_{wb} = -3.9$ cm^{-1}, and $g = 1.80$, and the fit is shown as a solid line in Figure 5. Using these values and eq 8, the ground state is determined to be an $S_T = {}^5/_2$ state arising from $S_{13} = 2$ and $S_{24} = {}^9/_2$, i.e., ($^5/_2$, 2, $^9/_2$) using the format (S_T, S_{13}, S_{24}). The first and second excited states are the ($^7/_2$, 1, $^9/_2$) and ($^3/_2$, 3, $^9/_2$) states at 6.1 and 12.3 cm^{-1}, respectively, above the ground state.

As can be seen in Table 8, the obtained J_{bb} and J_{wb} values for **2** are within the range expected for manganese(II/III) complexes bridged by μ_3-O^{2-} ions. The J_{bb} value (−9.2 cm^{-1}) is within the range (−2.8 to −24.6 cm^{-1}) observed for other [Mn^{III}(μ_3-O)$_2$$Mn^{III}$] units; interestingly, there is a distinct difference in J_{bb} values when the wingtip atoms are Mn^{III} (−21.9 to −24.6 cm^{-1}) compared with the case when they are Mn^{II} (−2.8 and −3.1 cm^{-1}), and the $J_{bb} = -9.2$ cm^{-1} value for **2** (wingtip atoms both Mn^{II} and Mn^{III}) is intermediate (although not midway) between these two types. The obtained J_{wb} value for **2** (−3.9 cm^{-1}) may be considered an average of the J_{wb} (Mn^{II}/Mn^{III}) and J'_{wb} (Mn^{III}/Mn^{III}) parameters for the molecule (Scheme 1), and the obtained value is within the ranges for both these types of interactions, −1.5 to −6.5 cm^{-1} and −2.7 to −10.2 cm^{-1}, respectively.

$(NBu^n_4)_2[Mn_8O_4(O_2CPh)_{12}(Et_2mal)_2(H_2O)_2]$ (5). As stated earlier, the $[Mn_8O_4]^{14+}$ core of **5** (Figure 3) can be conveniently described as two linked $[Mn_4O_2]^{7+}$ units. The exchange interaction within each of these units is analogous to that in **2** and is depicted in Scheme 1. Even assuming that $J_{wb} = J'_{wb}$, however, the greater complexity of the linked-butterfly structure precludes the application of the Kambe vector coupling method. The large number of metal atoms and the low-symmetry topology of the core mean that the spin Hamiltonian describing all the possible pairwise interactions cannot be transformed into an appropriate and equivalent form for which the eigenvalues can be obtained by inspection. Further, the complexity of the molecule rules out the matrix diagonalization method as a viable alternative approach. However, the structure of complex **5** suggests an assumption that would dramatically simplify the magnetochemical analysis and allow at least some insight into the nature of the complex: the two bonds (Mn(1)−O(6′) and Mn(1′)−O(6)) linking the two $[Mn_4O_2]^{7+}$ units of the $[Mn_8O_4]^{4+}$ core lie on the JT elongation axes of Mn(1) and Mn(1′), as already mentioned, and are consequently longer (2.258(10) Å) than the other Mn^{III}−oxide bonds (1.867(9)−1.902(10) Å). It is thus considered likely that exchange interactions *between* the halves of the molecule will be very weak and that, to a first approximation, the octanuclear core may be considered as two independent, noninteracting halves. With this assumption, the analysis of the χ_m *vs* T data for **5** parallels that for **2**. In Figure 6 is shown the effective magnetic moment of **5** plotted as μ_{eff} per $[Mn_8O_4]^{14+}$ and per $[Mn_4O_2]^{7+}$ subcore; the solid line is a fit of these data to the same theoretical expression employed to fit the χ_m *vs* T data for **2**. Only data for temperatures ≥40 K were employed, because at lower temperatures the weaker inter-$[Mn_4O_2]^{7+}$ interactions would assume greater importance; zero-field-splitting effects also become more important at lower temperatures. As can be seen in Figure 6, the agreement

(48) Tsai, H.-L.; Wang, S.; Christou, G.; Hendrickson, D. N. Unpublished results.
(49) Kambe, K. *J. Phys. Soc. Jpn.* **1950**, *5*, 48.

Table 8. Comparison of Exchange Parameters in μ_3-Oxide-Bridged Manganese(II/III) Complexes

complex	oxidn state	J_{bb}, cm^{-1} $Mn^{III}(\mu_3\text{-}O)_2Mn^{III}$	J_{wb}, cm^{-1} $Mn^{III}(\mu_3\text{-}O)Mn^{III}$	J_{wb}, cm^{-1} $Mn^{III}(\mu_3\text{-}O)Mn^{II}$	ref
$[Mn_4O_2(O_2CMe)_7(bpy)_2]^+$	$4Mn^{III}$	−23.5	−7.8		15
$[Mn_4O_2(O_2CMe)_7(pic)_2]^-$	$4Mn^{III}$	−24.6	−5.3		16
$Mn_4O_2(O_2CMe)_6(py)_2(dbm)_2$	$4Mn^{III}$	−21.9	−5.6		48
$[Mn_3O(O_2CMe)_6(py)_3]^+$	$3Mn^{III}$		−10.2		40
$Mn_4O_2(O_2CMe)_6(bpy)_2$	$2Mn^{II},2Mn^{III}$	−3.1		−2.0	15
$Mn_4O_2(O_2CCPh_3)_6(Et_2O)_2$	$2Mn^{II},2Mn^{III}$	−2.8		−1.5	34b
$Mn_3O(O_2CMe)_6(py)_3$	$Mn^{II},2Mn^{III}$		−2.7	−5.2	31
$Mn_3O(O_2CPh)_6(py)_2(H_2O)$	$Mn^{II},2Mn^{III}$		−4.5	−6.5	31

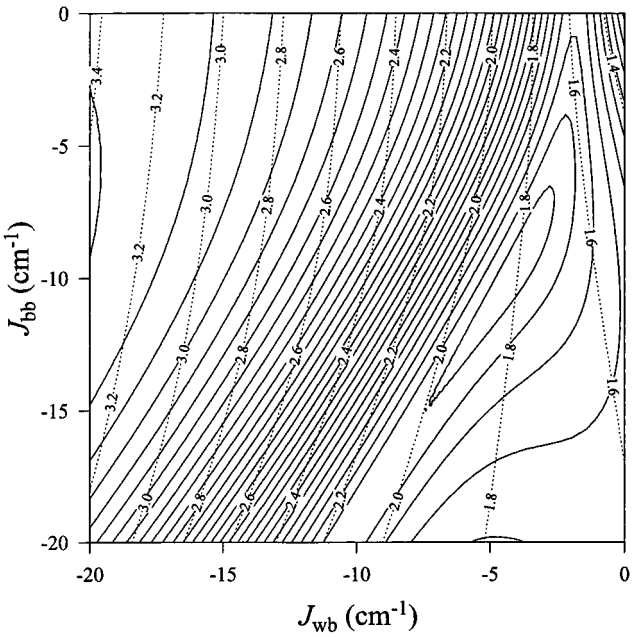

Figure 7. Two-dimensional contour projection of the rms error surface for $[Mn_4O_2(O_2CPh)_7(bpy)_2]$ (**2**). Also shown are the contours for the g value (dashed lines).

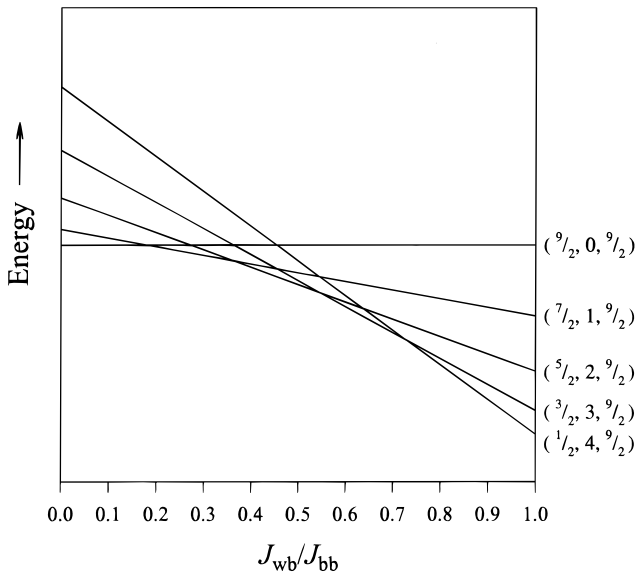

Figure 8. Variation in energy of the low-lying spin states of $[Mn_4O_2(O_2CPh)_7(bpy)_2]$ (**2**) as a function of J_{wb}/J_{bb}, showing the change in ground state.

between the experimental and calculated (solid line) values is reasonable for temperatures ≥40 K, but there is a sharp divergence below this temperature assignable to the approximations of the model employed and ZFS effects. The fitting parameters were $J_{bb} = -30.5$ cm^{-1} and $J_{wb} = -14.0$ cm^{-1}, with g held fixed at 1.93 (*vide infra*); a constant TIP term of 800×10^{-6} cm^3 mol^{-1} was also employed. As for complex **2**, the obtained J_{bb} and J_{wb} values indicate the ground state of the $[Mn_4O_2]^{7+}$ subcores of **5** to be the ($^5/_2$, 2, $^9/_2$) state, i.e., $S_T = {}^5/_2$.

In view of our previous experience[16] that both global and local minima may be encountered in fits of data for $[Mn_4O_2]$ complexes, a question arose as to the reliability of the conclusions regarding the ground states of **2** and the subcore of **5**. This point was addressed by consideration of the error surface diagrams for the two fits. For complex **2**, the relative error surface was generated as a function of J_{wb} and J_{bb} (0.0 to −20.0 cm^{-1} for each parameter); for given J_{wb} and J_{bb}, the g value was optimized and the root-mean-square error σ was calculated using eq 9, where n is the number of data points. The obtained

$$\sigma = \left[\frac{\sum(\chi_{calcd} - \chi_{exptl})^2}{n}\right]^{1/2} \quad (9)$$

error surface is shown as a two-dimensional contour projection in Figure 7 (solid lines); a contour plot of the optimized g value is also included (dashed lines). The error surface shows only a single minimum, within a shallow "valley" ($\sigma \leq 0.001$) suggestive of a poorly-defined minimum in the region $J_{bb} = -8$ to -12 cm^{-1}, $J_{wb} = -3$ to -6 cm^{-1}, and $g = 1.75-1.9$, with the minimum error being at $J_{bb} = -9.2(1)$ cm^{-1}, $J_{wb} = -3.9(1)$ cm^{-1}, and $g = 1.796(9)$ but other points in the indicated (J_{bb}, J_{wb}, g) range having only slightly greater relative error values. However, it is important to note that although the absolute magnitudes of J_{wb} and J_{bb} are poorly defined by the error surface, the value of J_{wb}/J_{bb} (i.e. the *relative* magnitude of J_{wb} *vs* J_{bb}) is *well* defined, being almost invariant at $J_{wb}/J_{bb} = 0.43 \pm 0.03$. The important question is thus to what extent the ground state of **2** is sensitive to the J_{wb}/J_{bb} ratio, given the above uncertainty in the value of this ratio. This is addressed in Figure 8, which shows the result of a calculation of the ground state S_T value as a function of the J_{wb}/J_{bb} ratio; the $S_T = {}^5/_2$ state is the ground state for J_{wb}/J_{bb} values in the range 0.36−0.54. Thus, the experimentally-determined value of 0.43 ± 0.03 is well within this range. Similarly, in Figure 9 is shown the $\sigma = 0.001$ error contour from Figure 7 projected onto a plot of ground state spin boundaries as a function of J_{wb} and J_{bb}. Using this contour as a guide to the location of all reasonable fits and noting that the long axis of the contour is parallel to that of the $S = {}^5/_2$ region, we can conclude that the fitting procedure has correctly identified the global minimum and that uncertainties in the absolute magnitudes of J_{wb}, J_{bb}, and g do not affect the conclusion that **2** has an $S_T = {}^5/_2$ ground state.

A similar consideration of the error surface for **5** (not shown) leads to the analogous conclusion that the fitting procedure identified the region of the global minimum. The point of minimum error is again poorly defined within an elongated $\sigma = 0.001$ error contour spanning the ranges $J_{bb} \approx -25$ to -40

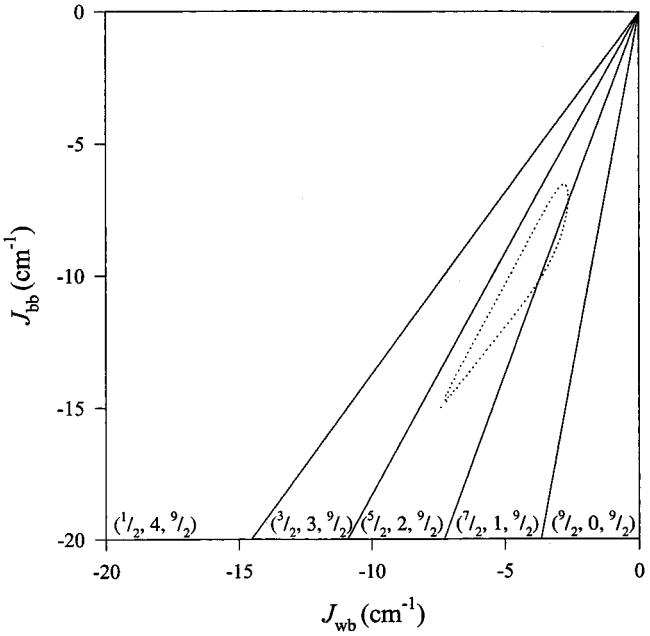

Figure 9. Plot of the ground state spin boundaries for $[Mn_4O_2(O_2CPh)_7(bpy)_2]$ (**2**) as a function of the J_{bb} and J_{wb} parameters. Shown as a dashed line is the $\sigma = 0.001$ contour from Figure 7.

cm^{-1} and $J_{wb} \approx -10$ to -20 cm^{-1} for $g = 1.8-2.0$, respectively. For this reason, a fixed g of 1.93 was employed for J_{bb} and J_{wb} determinations, this value of g having being obtained from the $M/N\mu_B$ *vs* H/T fits (*vide infra*) and thus considered to be reliable.

Magnetization *vs* Field Studies. In view of the assumptions inherent in the model used to fit the data for **2** (i.e. $J_{wb} = J'_{wb}$), magnetization *vs* field studies were performed to provide additional support for the $S_T = {}^5/_2$ ground state assignment. For complex **5**, the above treatment had assumed that the halves of the anion were only weakly interacting and an assessment of the spin of each half had been carried out: however, the spin of the ground state of the *whole* anion was not available from this treatment, and magnetization *vs* field studies on **5** were therefore performed to address this point. Data were collected for **2** and **5** in the 2−30 K range at field (H) values of 0.5, 1.0, 2.0, 3.0, 5.0, and 10.0 kG. The data for **2** and **5** are plotted in Figures 10 and 11, respectively as reduced magnetization ($M/N\mu_B$) *vs* H/T, where N is Avogadro's number and μ_B is the Bohr magneton.

For **2**, if the $S_T = {}^5/_2$ ground state were the only one populated at low temperatures and there was no zero-field splitting (ZFS), the various isofield lines would be superimposed and saturate at an $M/N\mu_B$ value of gS_T, i.e. 5 for $g = 2.0$ and $S_T = {}^5/_2$. In Figure 10, it can be seen that the lines do not superimpose, indicating the presence of ZFS, and that, at the highest H and lowest T values, the reduced magnetization is almost saturated at a value of ∼4.3; this is consistent with an $S_T = {}^5/_2$ ground state and a g value <2, as expected for Mn. We conclude that **2** does indeed have an $S_T = {}^5/_2$ ground state.

Figure 11 shows the $M/N\mu_B$ *vs* H/T data for **5** in the 2.00−4.00 K range, and it is clear that ZFS effects are significant and that the reduced magnetization has not reached saturation. The data were fit by diagonalization of the spin Hamiltonian matrix incorporating axial ZFS (DS_z^2) and Zeeman interactions and assuming only the ground state to be occupied at these temperatures. The solid lines in Figure 11 show that a good fit was obtained, with fitting parameters $S_T = 3$, $g = 1.93$, and $D = 4.92$ cm^{-1}. Thus, although the χ_m *vs* T studies at ≥40 K suggest that each half of the anion has an $S_T = {}^5/_2$ ground state,

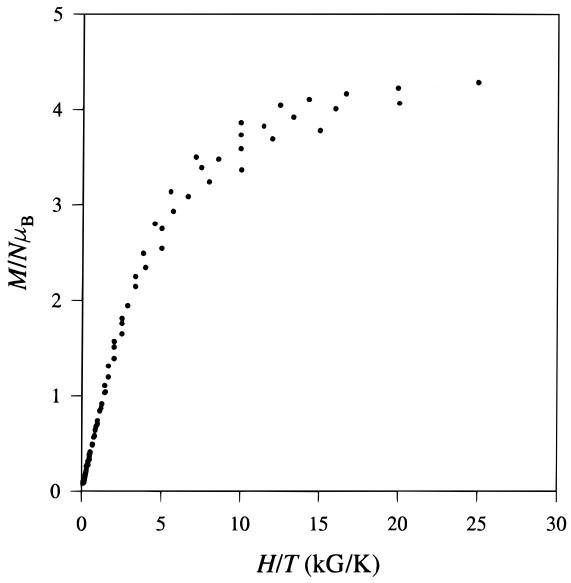

Figure 10. Plot of the reduced magnetization ($M/N\mu_B$) *vs* H/T for $[Mn_4O_2(O_2CPh)_7(bpy)_2]$ (**2**).

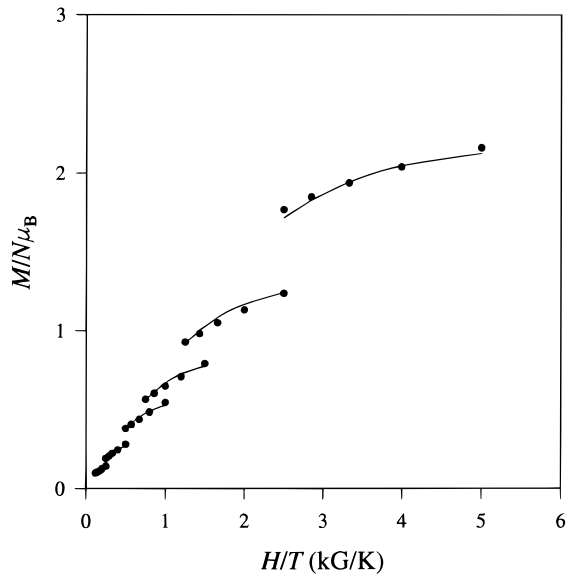

Figure 11. Plot of the reduced magnetization ($M/N\mu_B$) *vs* H/T for $(NBu^n_4)_2[Mn_8O_2(O_2CPh)_{12}(Et_2mal)_2(H_2O)_2]$ (**5**) in the 2.00−4.00 K and 0.5−10 kG ranges. The solid lines are fits of the data; see the text for details and fitting parameters.

the interactions between the halves yield an overall $S_T = 3$ ground state for the complete anion.

Origin of the $S_T = {}^5/_2$ Ground State. The identification of an $S_T = {}^5/_2$ ground state for the $Mn^{II},3Mn^{III}$ complex **2** is of interest *vis-à-vis* the previous determinations of $S_T = 3$ ground states for the $[Mn_4O_2(O_2CR)_7(L\text{-}L)_2]^z$ complexes (L-L = bpy, $z = +1$; L-L = pic$^-$, $z = -1$) with the same $[Mn_4O_2]$ butterfly core but at a higher oxidation state, i.e. $4Mn^{III}$. Our previous, detailed analyses of the exchange interactions within these complexes had identified the presence of spin frustration effects. Spin frustration may be defined in a general sense as the presence within certain topological arrangements of paramagnetic centers of competing exchange interactions, none of which dominates, that prevent (frustrate) the spin alignments that would otherwise be preferred in the ground state. For the oxidized ($4Mn^{III}$) butterfly complexes, J_{wb} and J_{bb} are both negative, but it is clearly impossible for the spins of each Mn^{III} center to be aligned antiparallel to each of the three neighboring spins. Such a situation leads to the ground state becoming particularly

Scheme 2

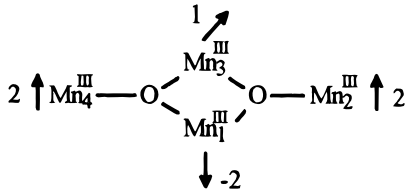

Scheme 3

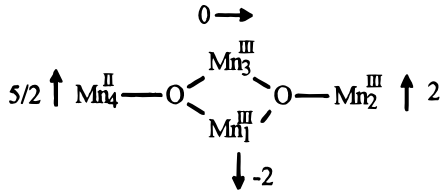

sensitive to the relative magnitudes of the competing interactions (i.e. the J_{wb}:J_{bb} ratio), and the spin of the ground state adopts an intermediate value ($S_T = 3$) rather than the low value ($S_T = 0$) that might be predicted for a completely antiferromagnetically-coupled system. The $S_T = 3$ ground state has $S_{13} = 1$ and $S_{24} = 4$ (using the labeling scheme employed for **2** for convenience), and this can be represented as in Scheme 2: this shows that the competing J_{wb} interactions prevent S_{13} from being zero, as expected, but instead an intermediate value, $S_{13} = 1$, which then aligns antiparallel to $S_{24} = 4$ to give the overall $S_T = 3$ ground state. Note that although J_{bb} is stronger than J_{wb} (Table 8), it does not dominate; there is only one of the former, and there are four of the latter.

It is thus of interest to attempt to rationalize the $S_T = {}^5/_2$ ground state as a perturbation of the $4Mn^{III}$ case above caused by addition of one electron to a wingtip Mn atom. Both J_{wb} and J_{bb} are still negative and **2** will thus still exhibit spin frustration, but what changes noticeably is the J_{bb}/J_{wb} value which is $-9.2/-3.9$ for **2** compared with (-21.9 to -23.5)/(-5.3 to -7.8) for the $4Mn^{III}$ complexes (Table 8). The J_{bb} interaction is thus weaker relative to that of J_{wb}. This rationalizes the $S_T = {}^5/_2$ ground state for **2**, which has $S_{13} = 2$ and $S_{24} = {}^9/_2$ and can be represented in Scheme 3: with J_{bb} relatively weaker, even the near-antiparallel alignment of S_1 and S_3 in Scheme 2 to give $S_{13} = 1$ is prevented by the J_{wb} interactions, and this value is now $S_{13} = 2$ in **2** (Scheme 3), which aligns antiparallel to $S_{14} = {}^9/_2$ to give the observed $S_T = {}^5/_2$ ground state. Thus, the significant weakening of the J_{bb} interaction on reduction of a wingtip Mn^{III} ion appears to be the main factor responsible for the $S = {}^5/_2$ ground state of **2**; had the relative J_{bb} and J_{wb} values remained as they are in the $4Mn^{III}$ complexes, the ground state of **2** would have been expected to be $S_T = {}^9/_2 - 1 = {}^7/_2$.

For **5**, the above arguments and Scheme 3 rationalize the $S = {}^5/_2$ state of each half of the anion deduced from the ≥ 40 K data. Note that the J_{bb} and J_{wb} values (-30.5 and -14.0 cm^{-1}, respectively) again indicate a strengthening of J_{wb} relative to J_{bb}. The presence of the weaker *inter*fragment interactions (both through the central bridging oxygen atoms, O(6) and O(6′), and *via* the bridging Et_2mal^{2-} ligands) and resulting additional spin frustration effects give an $S_T = 3$ ground state for the entire molecule, but this is not easy to rationalize further in a simple, qualitative manner.

EPR Spectroscopy. The X-band EPR spectra for complex **2** were recorded in a CH_2Cl_2/toluene (1:1) glass at temperatures from 4.7 to 60 K (Figure 12); complex **5** is EPR silent. At 4.7 K, four features are adequately resolved with g values of ∼2.0, ∼3.0, ∼5.2, and ∼8.2. The intensity of the $g = 5.2$ signal decreases rapidly with increasing temperature; the intensity of the $g \approx 2.0$ feature remains relatively constant until 30 K and then decreases. No signals were observed at 78 K. In view of the broadness and poor resolution of the EPR features, no analysis of the spectrum has been pursued.

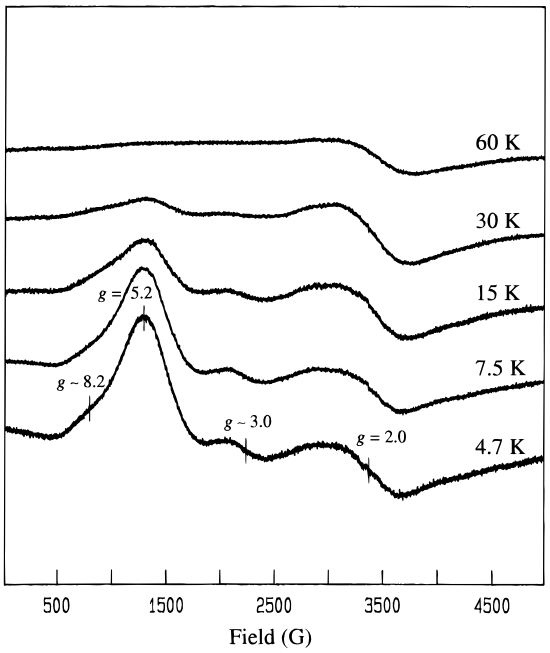

Figure 12. X-band EPR spectra of $[Mn_4O_2(O_2CPh)_7(bpy)_2]$ (**2**) in a CH_2Cl_2/toluene (1:1) glass at the indicated temperatures.

Summary and Conclusions. The reaction of Et_2mal^{2-} with complex **4**, a highly convenient source of the $[Mn_4O_2]^{8+}$ unit, provides a good route to the new, mixed-valence ($2Mn^{II}$,$6Mn^{III}$) octanuclear complex **5**. The core of the latter can be considered two $[Mn_4O_2]^{7+}$ units linked together, with the Mn^{II} ions in two of the four wingtip positions. Each of the $[Mn_4O_2]^{7+}$ subcores corresponds to that of $[Mn_4O_2(O_2CR)_7(bpy)_2]$ (**2**) and supports the latter also having the Mn^{II} at a wingtip position. It is interesting to note that both **2** and the $[Mn_4O_2]^{7+}$ subcore of **5** have $S = {}^5/_2$ ground states, and this can be readily rationalized by consideration of the relative magnitudes of the exchange interactions and the resulting spin frustration effects. Such considerations are also finding useful application in rationalizing the variation in ground state spin values for the $[M_4O_2(O_2CR)_7(bpy)_2]^+$ ($M = V^{III}$, Cr^{III}, Mn^{III}, Fe^{III}) series of complexes, and this will be reported in due course. Complex **5** is a new addition to the growing family of high-nuclearity carboxylate clusters, and it has a ground state spin of $S_T = 3$, providing a useful new datum point for the ongoing objective of understanding the ground state spin value of transition metal carboxylate clusters as a function of metal, oxidation state, and topology of the polynuclear metal core.

Acknowledgment. This work was supported by the National Institutes of Health (Grant GM 39083) and the National Science Foundation (Grants CHE-9420322 and CHE-9311904).

Supporting Information Available: Text summarizing the data collection and structure solutions, tables listing crystal and diffractometer data, fractional coordinates, anisotropic thermal parameters, and bond distances and angles, and fully labeled figures for complexes **4**, **5**, and **7** (70 pages). Ordering information is given on any current masthead page.

IC9603013